Bioactive Materials 26 (2023) 292–305

Contents lists available at ScienceDirect

Bioactive Materials

journal homepage: www.keaipublishing.com/en/journals/bioactive-materials

Functionalization of *in vivo* tissue-engineered living biotubes enhance patency and endothelization without the requirement of systemic anticoagulant administration

Hongyu Yan [a,b,1], Quhan Cheng [a,1], Jianghua Si [a], Songdi Wang [a], Ye Wan [a], Xin Kong [a], Ting Wang [c], Wenting Zheng [d], Muhammad Rafique [a], Xiaofeng Li [e], Ju He [e], Adam C. Midgley [a,**], Yi Zhu [f], Kai Wang [a,*], Deling Kong [a]

[a] Key Laboratory of Bioactive Materials for the Ministry of Education, College of Life Sciences, Nankai University, Tianjin, 300071, China
[b] Department of Ultrasound in Medicine, Shanghai Sixth People's Hospital Affiliated to Shanghai Jiao Tong University School of Medicine, Shanghai, 200233, China
[c] Tianjin Key Laboratory of Urban Transport Emission Research, College of Environmental Science and Engineering, Nankai University, Tianjin, 300071, China
[d] State Key Laboratory of Experimental Hematology, National Clinical Research Center for Blood Diseases, Chinese Academy of Medical Sciences & Peking Union Medical College, Tianjin, 300020, China
[e] Department of Vascular Surgery, Tianjin First Central Hospital, Nankai University, Tianjin, 300192, China
[f] Department of Physiology and Pathophysiology, Tianjin Medical University, Tianjin, 300070, China

ARTICLE INFO

Keywords:
In vivo tissue-engineering
Biotube
Living tissue modification
Anticoagulation
Rapid endothelialization

ABSTRACT

Vascular regeneration and patency maintenance, without anticoagulant administration, represent key developmental trends to enhance small-diameter vascular grafts (SDVG) performance. *In vivo* engineered autologous biotubes have emerged as SDVG candidates with pro-regenerative properties. However, mechanical failure coupled with thrombus formation hinder translational prospects of biotubes as SDVGs. Previously fabricated poly (ε-caprolactone) skeleton-reinforced biotubes (PBs) circumvented mechanical issues and achieved vascular regeneration, but orally administered anticoagulants were required. Here, highly efficient and biocompatible functional modifications were introduced to living cells on PB lumens. The 1,2-dimyristoyl-*sn*-glycero-3-phosphoethanolamine-N-methoxy (DMPE)-PEG-conjugated anti-coagulant bivalirudin (DPB) and DMPE-PEG-conjugated endothelial progenitor cell (EPC)-binding TPS-peptide (DPT) modifications possessed functionality conducive to promoting vascular graft patency. Co-modification of DPB and DPT swiftly attained luminal saturation without influencing cell viability. DPB repellent of non-specific proteins, DPB inhibition of thrombus formation, and DPB protection against functional masking of DPT's EPC-capture by blood components, which promoted patency and rapid endothelialization in rat and canine artery implantation models without anticoagulant administration. This strategy offers a safe, facile, and fast technical approach to convey additional functionalization to living cells within tissue-engineered constructs.

1. Introduction

Small-diameter vascular grafts (SDVGs) fabricated with synthetic materials, such as expanded poly(tetraflouroethylene) (ePTFE) and poly (ethylene terephthalate) (PET), often fail due to thrombosis and intimal hyperplasia [1]. Tissue engineered vascular grafts (TEVGs) demonstrate superior regenerative properties and have emerged as promising SDVGs candidates [2,3]. However, incidence of acute thrombosis, comprised of fibrin and platelet aggregates that form at the blood-material interface, has hindered the clinical uptake of TEVGs [4–6]. Systemic administration of antiplatelet drugs, anticoagulants, or a combination of both, are often employed in clinical settings to inhibit thrombosis, but come with increased risks of adverse bleeding [7,8]. Strategies to functionalise the TEVG blood-interfacing surface can offer potential routes towards

Peer review under responsibility of KeAi Communications Co., Ltd.
* Corresponding author.
** Corresponding author.
E-mail addresses: midgleyac@nankai.edu.cn (A.C. Midgley), 013053@nankai.edu.cn (K. Wang).
[1] These authors contributed equally to this work.

https://doi.org/10.1016/j.bioactmat.2023.03.003
Received 15 December 2022; Received in revised form 19 February 2023; Accepted 5 March 2023

minimizing activation of blood components, producing anti-thrombotic effects, and reducing the need for administration of anticoagulant drugs.

Strategies to improve TEVG hemocompatibility have utilized passive approaches, such as the incorporation of zwitterionic components [9,10], polyethylene glycol (PEG) decoration [11,12], and other molecular modifications [13,14], which were shown to inhibit thrombus formation by improving resistance against platelet and plasma protein adhesion. Despite improved hemocompatibility results *in vitro*, such passive approaches have proven ineffective in obtaining long-term hemocompatibility *in vivo* [15]. This may be explained by inadvertent masking of endothelial cell (EC) and endothelial precursor cell (EPC) recruitment, thereby hindering re-endothelialization [16,17]. The endothelium prevent thrombus formation and inhibits intimal hyperplasia through regulating vascular smooth muscle cell (VSMC) proliferation [18]. Therefore, ideal blood-interfacing surfaces should be capable of conveying anticoagulation activity whilst inducing timely endothelialization, to achieve heightened patency.

Capture of circulating EPCs *in situ* was shown to promote endothelialization and represents a practical strategy in comparison to pre-seeding scaffolds with ECs [19]. Graft modifications with biological ligands that possess high affinity for EPC binding (e.g., antibodies, aptamers, and polypeptides) have demonstrated active capture and recruitment of EPCs [20–22]. Compared to other ligands, polypeptides have advantages in their facile synthesis, purification, storage, and controllable bioactivity [23,24]. The polypeptide, TPSLEQRTVYAK (TPS), has been shown to exhibit high affinity and binding specificity for EPCs in multiple experimental models across multiple species, including mouse [25], rat [26,27], canine [27,28]and human [29] studies. Furthermore, TPS had no negative effect on proliferation, migration, or tube formation of EPCs [30]. Therefore, TPS represents an ideal polypeptide ligand for EPC capture [31,32].

Pro-endothelialization graft modification technologies have rarely been reported in large animal pre-clinical studies or in clinical studies [33,34]. A potential reason for invalidity of surface functional modification is the unspecific adhesion of plasma proteins [35,36]. Fibrinogen (FIB) is quickly adsorbed onto blood-material interfaces, thus masking activity of pro-endothelialization molecules and concomitantly promotes platelet aggregation and thrombus formation [6,37]. Heparin is frequently employed as an anticoagulant in clinical practice and has been widely adopted for modification of TEVGs [38,39]. Heparin binds to antithrombin but also non-specifically binds to other plasma proteins, such as fibronectin and growth factors [40,41]. Additionally, heparin is susceptible to inactivation by platelet factor 4 (PF4) released by activated platelets [42]. Such non-specific interactions may reduce heparin's anti-coagulation activity at the TEVG surface, resulting in unsatisfactory outcomes [43,44]. Thrombin's catalysis of FIB to fibrin [45] has made it a major target of many anticoagulants. The synthetic short peptide bivalirudin (BVLD) is a highly-efficient and specific thrombin inhibitor [46], which directly inhibits FIB recognition and its catalysis by thrombin [47], inhibits thrombin mediated platelet adhesion and activation, and is not susceptible to inactivation by PF4 [48]. Thus, BVLD serves as an attractive molecule for TEVG modification, to realise anticoagulant function whilst effectively protecting co-modified molecules against loss of function resulting from obscuration by FIB and platelets.

In vivo tissue engineering exploits the foreign body response (FBR) to implanted materials and can be used to fabricate autologous TEVGs [49,50]. Previously, we fabricated polymer-reinforced biotubes (PBs) by subcutaneous implantation (SI) of melt-spun poly(ε-caprolactone) (PCL) fiber skeletons [51]. PBs circumvented issues relating to insufficient mechanical strength that is typically encountered by traditional biotubes consisting only of autologous tissue [52]. Our PBs excelled in their demonstratable biomechanical, biodegradable and vascular regeneration properties, but their implantation in canine arterial replacement models required oral anticoagulant drugs to be administered throughout the implantation period to maintain patency [51]. Therefore, we hypothesise that modifying PBs to improve hemocompatibility can eliminate the need for administration of anticoagulant drugs in large animal models.

Conventional modification methods, such as covalent crosslinking, layer-by-layer self-assembly, or electrostatic interactions are less suitable for the modification of bioactive molecules onto the blood-interfacing surface of living tissue PBs, primarily due to time-expensive methodology and varying degrees of cytotoxicity [53]. We previously utilized hydrophobic interactions between polypeptide-linked PEG-conjugated phospholipids (DMPE-PEG) and the phospholipid bilayer of the cell membrane to successfully incorporate functional polypeptides into the membrane of living cells without impairment of cell activity and function [54]. In this study, DMPE-PEG was covalently bonded to TPS (DPT) or BVLD (DPB) and both were co-modified onto the surfaces of living cells on the PB lumens (Scheme 1). DPB modifications were utilized to achieve a "kill three birds with one stone" strategy: (i) to improve hemocompatibility by inhibiting FIB and platelet adhesion; (ii) to decrease non-specific plasma protein adsorption due to PEG incorporation; and (iii) to protect DPT function through prevention of masking by blood components. We first optimized DPT:DPB co-modifications on PBs by *in vitro* assessment of biocompatibility, anticoagulation capacity, and capability to capture EPCs from dynamic flow culture. Next, we evaluated *in vivo* regenerative abilities in rat abdominal artery implantation models. The performance of optimized DPT/DPB-modified PBs was then further verified in canine carotid artery implantation models. The results shown here offer insights and reference for surface modification of vascular grafts and tissue-engineered constructs that contain living cells, and have broader implications in strategies of surface functional regulation for autologous tissues or transplanted organs.

2. Results and discussion

2.1. Fabrication of PBs and optimization of modification conditions

Subcutaneous implantation of our previously optimized melt spun PCL fiber skeleton [51] was re-employed in this study to generate PBs. Firstly, the optimized melt-spin preparation parameters were followed, and the resultant PCL fiber skeletons were morphologically characterized (Table S1 and Figs. S1a and b, Supporting Information). PBs were then prepared in rats and canine models (Figs. S1c and d, Supporting Information) by subcutaneous implantation of the PCL fiber skeletons for 30 days. PBs were comprised of PCL fiber skeletons that had autologous tissue occupying the spaces between the PCL fibers. Immunofluorescence staining revealed that the lumen surface of rat-derived PBs (inner diameter: 2 mm) and canine-derived PBs (inner diameter: 3.5 mm) were covered by α-smooth muscle actin-positive (α-SMA^{+}) cells (Figs. S1e and f, Supporting Information), which was in-line with our previous observations [51].

During the subcutaneous implantation time, DPT and DPB were synthesized and verified by ^{1}H NMR spectra (Fig. S2, Supporting Information). DPT was synthesized by Michael addition reaction between the carbon-carbon double bonds of DMPE-PEG-MAL and the sulfhydryl group of TPS (Fig. S2a, Supporting Information). In the spectra of DPT (Fig. S2b, Supporting Information), the presence of benzene ring group in tyrosine (6.8 ppm and 7.1 ppm) and the $–CH_2-$ characteristic peak (3.6 ppm) belonging to PEG in DMPE-PEG-MAL, indicated the successful synthesis of DPT. Based on the condensation reaction of primary amine groups and carboxyl groups, DMPE-PEG-NH_2 was covalently linked with carboxyl groups of BVLD (Fig. S2c, Supporting Information) to synthesize DPB. In the ^{1}H NMR spectra of DPB (Fig. S2d, Supporting Information), the characteristic peak (6.8 ppm and 7.1–7.3 ppm) assigned to the benzene ring of BVLD and the characteristic peak (3.6 ppm) belonging to $–CH_2-$ of DMPE-PEG-NH_2could be observed, indicating the successful synthesis of DPB.

We next sought to optimize the modification conditions

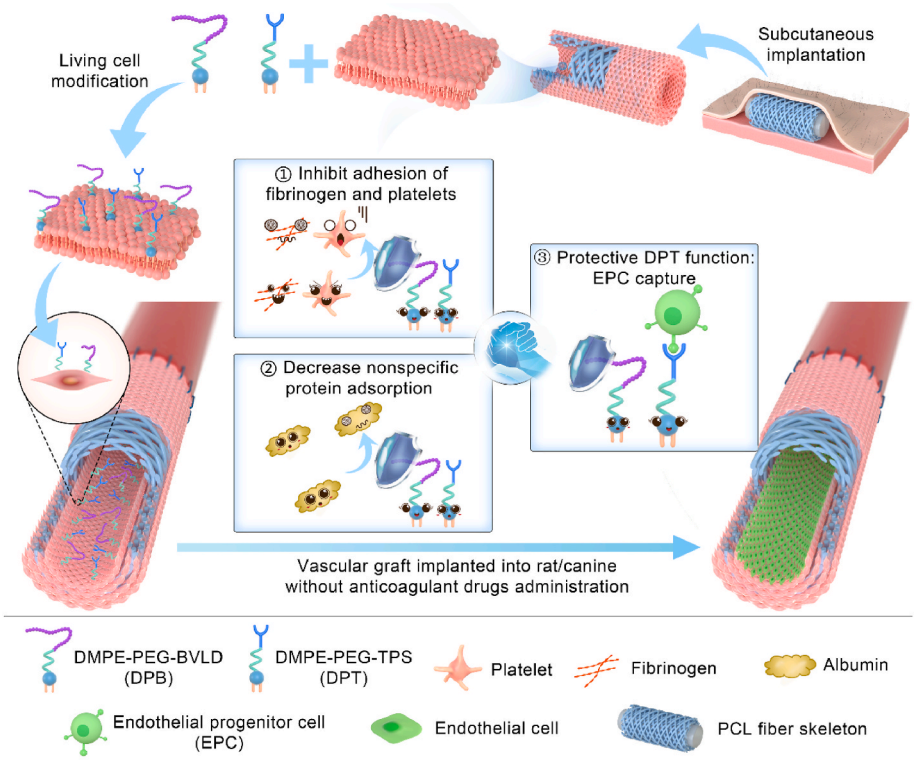

Scheme 1. DPB and DPT co-modified PB lumens. The lumens of *in vivo* engineered PBs were co-modified with DPB and DPT. The DPB modifications (1) boosted resistance against fibrinogen and platelet activation and aggregation, (2) reduced nonspecific protein absorption, and (3) protected DPT's EPC capture functionality against masking by blood components. Co-modifications improved PB patency rates and enhanced endothelialization of PBs in rat and canine arterial implant models, without requirement of anticoagulant drug administration.

(concentration and incubation time) of DMPE-PEG-conjugated peptides. In order to visualize the extent of modification, DMPE-PEG-Cy7 (DP-Cy7) was synthesized. PEG-Cy7 (P-Cy7) has a similar molecular structure to DP-Cy7 but lacks the lipid component, and was synthesized as a control to investigate the immobilization effect of DMPE within DP-Cy7. As shown in the schematic (Fig. 1a), PBs were incubated with the different concentrations of DP-Cy7 or P-Cy7. Following incubation for 10 min, the fluorescence signal of the whole PBs was assessed. Results showed that 5 μM DP-Cy7 modified PBs exhibited near complete fluorescence signal coverage, whereas P-Cy7 could not be visualized, even in the higher concentration 20 μM group (Fig. 1b). The mean fluorescence intensity (MFI) of DP-Cy7 modified PBs, as quantified by Indigo (Berthold Technologies) showed positive correlation with the DP-Cy7 concentration (Fig. 1c). The MFI plateaued at 15 μM DP-Cy7 and did not obviously increase further when utilizing 20 μM DP-Cy7. Confocal images and corresponding statistics showed that both 15 μM (98.17 ± 0.85%) and 20 μM DP-Cy7 (98.30 ± 1.19%) had almost labelled all cells of the PB lumen surface (Fig. 1d and e), which also verified that 15 μM DP-Cy7 was sufficient to achieve saturated modification. Notably, the fluorescence signal of DP-Cy7 was distinctly localized along the cell periphery, demonstrating that the DMPE component of DP-Cy7 had inserted into the cell membrane through hydrophobic interaction. Subsequently, the fluorescence signal of PBs modified with 15 μM DP-Cy7 for different incubation times was also assessed. The fluorescence signal of DP-Cy7 has sufficiently covered the lumen surfaces of PBs as rapidly as after 1 min incubation time (Fig. 1f). After incubation for 15 min, the 15 μM P-Cy7 group still demonstrated no detectable signal. Quantitative data indicated that the MFI of PBs modified with 15 μM DP-Cy7 at the 15 min time-point was comparable with that at the 10 min time-point (Fig. 1g), which indicated that the modification degree had reached saturation by 10 min. The fluorescence signal of the lumen surface of 15 μM DP-Cy7 modified PBs was observable by confocal microscopy after 5 min incubation, unlike the fluorescence signal of 15 μM P-Cy7, which remained undetectable at 15 min incubation time (Fig. 1h and i). The percentage of DP-Cy7 labelled cells on the lumen surface in the 15 μM modified PB group, as quantified from confocal microscopy images, showed no obvious increases at 15 min incubation (96.06 ± 1.70%) compared to at 10 min (97.19 ± 1.33%), which was similar to the trend exhibited by the quantified MFI data. These results suggested that incubation with 15 μM DP-Cy7 for 10 min was sufficient to saturate the PB lumens with DP-modifications. The cross sections and longitudinal sections of PBs modified with 15 μM DP-Cy7 for 10 min were observed using confocal microscopy (Fig. S3, Supporting Information). The fluorescence signal was uniformly and distinctly distributed on the lumen surface of PBs, which indicated that our method achieved lumen-specific modification.

Taken together, the data indicated the simplicity and time efficient modifications made with DMPE-PEG-conjugated molecules. The DP-based modifications lend themselves to clinical feasibility when preparing autologously generated tissue constructs; the methodology avoids complex external processes, and time-expensive preparation procedures. The optimized modifications demonstrated here were used for further experiments.

2.2. *Assessment of modification biocompatibility and stability*

As a product of the FBR, biotubes were reported to be enriched with fibroblastic cells [55]. These cells exhibit plasticity, can acquire contractile VSMC-like characteristics, and play key roles in matrix synthesis and remodelling after vascular grafting [52,56]. Thus, it is important to maintain cell viability throughout the modification process. The biocompatibility of DMPE-PEG-conjugated peptide modifications was primarily evaluated. The prepared PBs were divided into five groups to incubate for 10 min with different DPT: DPB concentration. The groups were as follows: (i) unmodified PBs; (ii) 15 μM DPT modified PBs (15 μM DPT-PBs); (iii) 10 μM DPT + 5 μM DPB modified PBs (10 μM DPT + 5 μM DPB-PBs); (iv) 7.5 μM DPT + 7.5 μM DPB modified PBs (7.5 μM DPT + 7.5 μM DPB-PBs); and (v) 5 μM DPT + 10 μM DPB modified PBs (5 μM DPT + 10 μM DPB-PBs). PBs incubated with 0.1% Triton X-100 for 10 min were used as positive controls to induce cell lysis [57]. Live/Dead staining revealed that the vast majority cell on the lumen surface of PBs modified with DPT/DPB were living, which was similar with unmodified

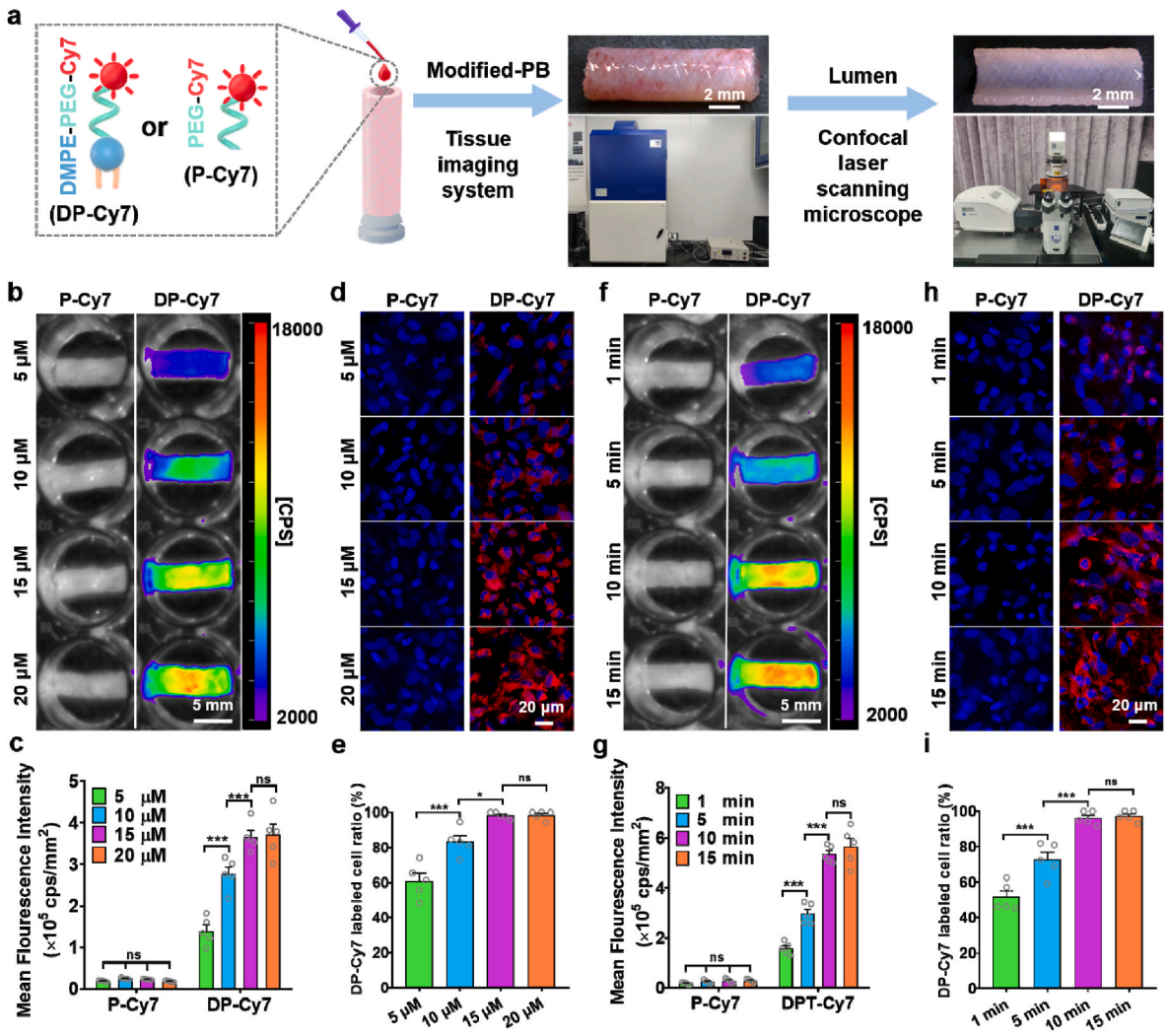

Fig. 1. Optimization of incubation conditions for DP-Cy7 modification of PBs. a) Schematic diagram of the P-Cy7 or DP-Cy7 modification of PB lumens. b) Representative fluorescence images and c) quantitative of mean fluorescence intensity (MFI) analysis of different concentrations of DP-Cy7 or P-Cy7 incubated with PBs for 10 min. d) Representative confocal micrographs of PB lumen after 10 min incubation with different concentrations of DP-Cy7 or P-Cy7. e) Quantification of DP-Cy7 labelled cells calculated based on confocal images. Five images per sample and five samples per group were used to obtain statistical results. f) Representative fluorescence images and g) quantitative MFI analysis of 15 μM DP-Cy7 or P-Cy7 incubated with PBs after different incubation times. h) Representative confocal micrographs of PB lumen after different incubation times with 15 μM DP-Cy7 or P-Cy7. i) DP-Cy7 labelled cells were quantified based on confocal images. Five images per sample and five samples per group were evaluated to obtain statistical results. For quantitative analyses, data are presented as the mean ± SEM (n = 5). Statistical significance is indicated as $^{*}P < 0.05$, $^{***}P < 0.001$, and ns: not significant, as determined by one-way analysis of variance (ANOVA) with Tukey's post hoc analysis.

PBs and in contrast to Triton X-100 treated PBs (Fig. 2a). In addition, CCK-8 assays confirmed that there were no obvious differences in cell metabolic activity between the modified and unmodified PBs (Fig. 2b), thereby indicating that modifications did not negatively affect cell number or cell viability. The expression of apoptosis-related genes (*Casp8*, *Casp9*, *Fas*, *Bax*, *Fasl, Bad*) and metabolism-related genes (*Glut1*, *Glut4*, *Ldha*, *Pgc1*, *Pkm2, Cs*) showed no significant differences between unmodified and modified PBs (Fig. 2c).

Several approaches including electrostatic interaction, covalent conjugation, and enzymatic ligation have already been successfully employed to modify living cell surfaces with exogenous bioactive molecules [58]. Indeed, these methods could potentially be utilized to modify the cells on the PB lumens. Instead, we opted for a simple and convenient method that would be more favourable in clinical applications, an approach that altogether avoids risks of cytotoxicity such as polycations (as in electrostatic interaction) [59], membrane proteins impairment (as in covalent coupling) [60], or restricted enzyme catalytic sites (as in enzymatic ligation) [61]. DMPE-PEG consists of a cell membrane-friendly component (DMPE) [62] and a biologically inert PEG chain, which has been widely used as an effective and biocompatible linker to anchor bioactive molecules to living cell surfaces without negatively impacting on cell viability [63]. Our own results supported that DMPE-PEG-conjugated peptide modifications exhibited the biocompatibility necessary for a method to safely modify PB lumens.

In consideration of exposure to blood flow shear stress and the complex *in vivo* environment after vascular implantation, the stability of the modified molecules on the graft lumen will ultimately affect the efficacy of the modifications. The stability of the DP-conjugated peptide modifications on the PB lumen surface was investigated based on fluorescence imaging technology. PBs modified with 15 μM DP-Cy7 for 10 min were linked in series, attached to a flow culture bioreactor, incubated at 37 °C and operational for up to 72 h (Fig. S4a, Supporting Information). The flow rate of serum-containing culture medium was set at 12.47 cm/s to simulate *in vivo* blood flow [64]. The fluorescence signal of DP-Cy7 gradually decreased over time without sudden losses in distinct areas (Fig. S4b, Supporting Information). The MFI of DP-Cy7

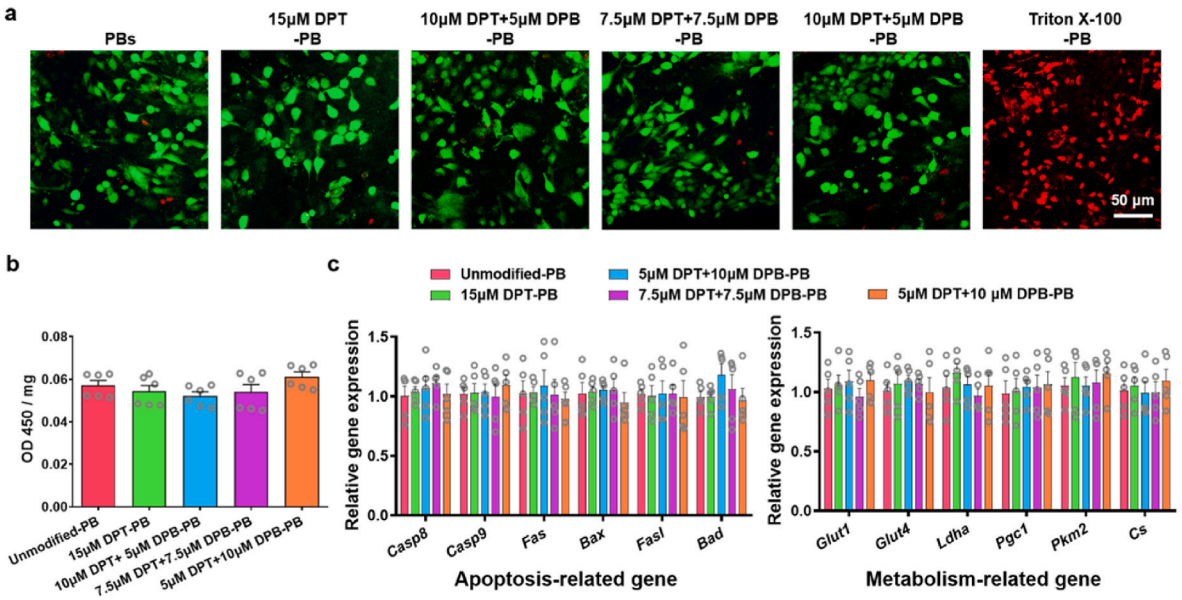

Fig. 2. The safety analysis of DPT/DPB modification for PBs. a) Representative Live/Dead fluorescence staining images of different DPT:DPB concentration modified onto PBs. PBs incubated with 0.1% Triton X-100 for 10 min were used as positive control for cell death. b) The cell viability of differentially DPT/DPB-modified PBs (n = 5). c) The relative expression of apoptosis-related genes and metabolism-related genes in differentially DPT/DPB-modified PBs (n = 5). For quantitative analyses, data are means ± SEM (n = 5) and there was no significance across the five groups, as determined by one-way ANOVA with Tukey's post hoc analysis.

modified PBs at 72 h post-flow culture was 30.88 ± 4.32% of the initial MFI (Fig. S4c, Supporting Information). PBs modified with 15 μM DP-Cy7 for 10 min were also implanted into rat abdominal artery replacement models to evaluate *in vivo* modification stability. Following implantation for 3 days, DP-Cy7 modified PBs exhibited a detectable fluorescence signal that was maintained at 28.57 ± 8.56% of the initial MFI (Figs. S4d and e, Supporting Information) and the fluorescence signal was still detectable after 7 days (17.80 ± 5.83% of the initial MFI). These results indicated that after modification with 15 μM DP-Cy7 for 10 min, DMPE-PEG-conjugated molecule modifications remained on the luminal surfaces of PBs for at least 7 days post-implant. Our results were similar to those shown in a series of works by Iwata et al. [65,66], wherein fluorescently-labelled PEG linked to lipid derivatives were used to modify islets cells' surfaces and remained detectable over 4–7 days *in vitro*.

2.3. Evaluation of DPT/DPB-modified PB hemocompatibility

Thrombus formation at the material-blood interface is triggered within minutes of blood exposure, primarily by the adhesion and activation of FIB and platelets [5]. The fibrin network formed from the cleavage of adhered FIB and the aggregation of activated platelets constitutes the backbone of the thrombus [67]. In this process, thrombin plays a crucial role, not only in converting fibrinogen to fibrin, but also by promoting platelet activation and aggregation [68]. Therefore, we primarily examined the inhibitory effect of DPT/DPB modification on thrombin activity (Fig. S5, Supporting Information). The results showed that the thrombin activity of 15 μM DPT-PBs group was comparable to that of unmodified-PB group, indicating that the only DPT modification had little effect on inhibiting thrombin activity. However, DPT and DPB co-modification effectively inhibited thrombin activity in a DPB concentration-dependent manner. Subsequently, we evaluated the capacity of modified-PB to inhibit fibrin network formation and platelet adhesion, which has been casually linked to improved patency of vascular grafts [69–71]. Alexa Fluor 488-labelled FIB was used to detect the FIB adhesion on differentially modified PBs via tissue imaging with a NightOWL LB983 Imaging System (Fig. 3a). The quantitative MFI analysis showed that all DPT and DPB co-modification conditions had demonstratable capacity to reduce FIB adhesion on the lumen surface of PBs. Whereas 15 μM DPT modification alone failed to produce a significant inhibitory effect on FIB adhesion, compared to unmodified PBs (Fig. 3b). Confocal images visualized the fibrin networks that had formed from the adhered FIB on PBs lumen (Fig. 3c). Dense networks composed of thin fibrin fibers covered the unmodified-PB and the 15 μM DPT-PB lumens, whereas a dispersed and coarse network of fibrin had formed on the lumens of DPT and DPB co-modified PBs. The inhibitory effect on FIB binding and fibrin formation correlated with increasing DPB modification concentration. FIB adhesion and polymerization was markedly reduced and only a few isolated fibrin fibers were observable on the lumens of the 5 μM DPT +10 μM DPB-PBs. Previous studies have shown that thrombin significantly impacts on fibrin network structure [72,73]. In the presence of a high concentration of thrombin, fibrin tends to produce dense networks; in contrast to this, dispersed coarse networks of fibrin become apparent in the presence of low thrombin concentrations [74]. The high affinity and specificity of BVLD binding to the active site of thrombin effectively inhibits thrombin activity [75]. In consideration of the crucial involvement of thrombin in fibrin network formation, it was unsuprising that the DPB consequently reduced FIB adhesion and fibrin network formation on the PB lumens. This suggested that DPT would remain unmasked and functional in the presence of co-modified DPB.

Typically, the extent of platelet activation can be evaluated according to the morphology of adhered platelets, and this can be used to assess a material's thrombogenicity [76]. Scanning electron microscopy (SEM) images showed that most of the platelets adhered to the lumen of unmodified PBs appeared multiple spread dendritic pseudopods (Fig. 3d, top row), indicative of platelets in an activated state [77]. The platelets adhered to the modified PBs tended to maintain the inactivated rounded morphology and fewer number with increasing DPB concentration. Next, mepacrine staining (Fig. 3d, middle layer images) and anti-CD62P immunofluorescence staining (Fig. 3d, lower layer images) were performed to quantify the adhesion and activation state of platelets on the differentially modified PB lumens, respectively. The effect of DPT/DPB co-modification on anti-platelet adhesion and activation was reflected by the quantitative data (Fig. 3e and f), which verified the observations made by SEM and showed the similar trend with resist FIB adhesion. This is because that in addition to BVLD dependent inhibition of thrombin induced fibrin network formation, it also suppresses

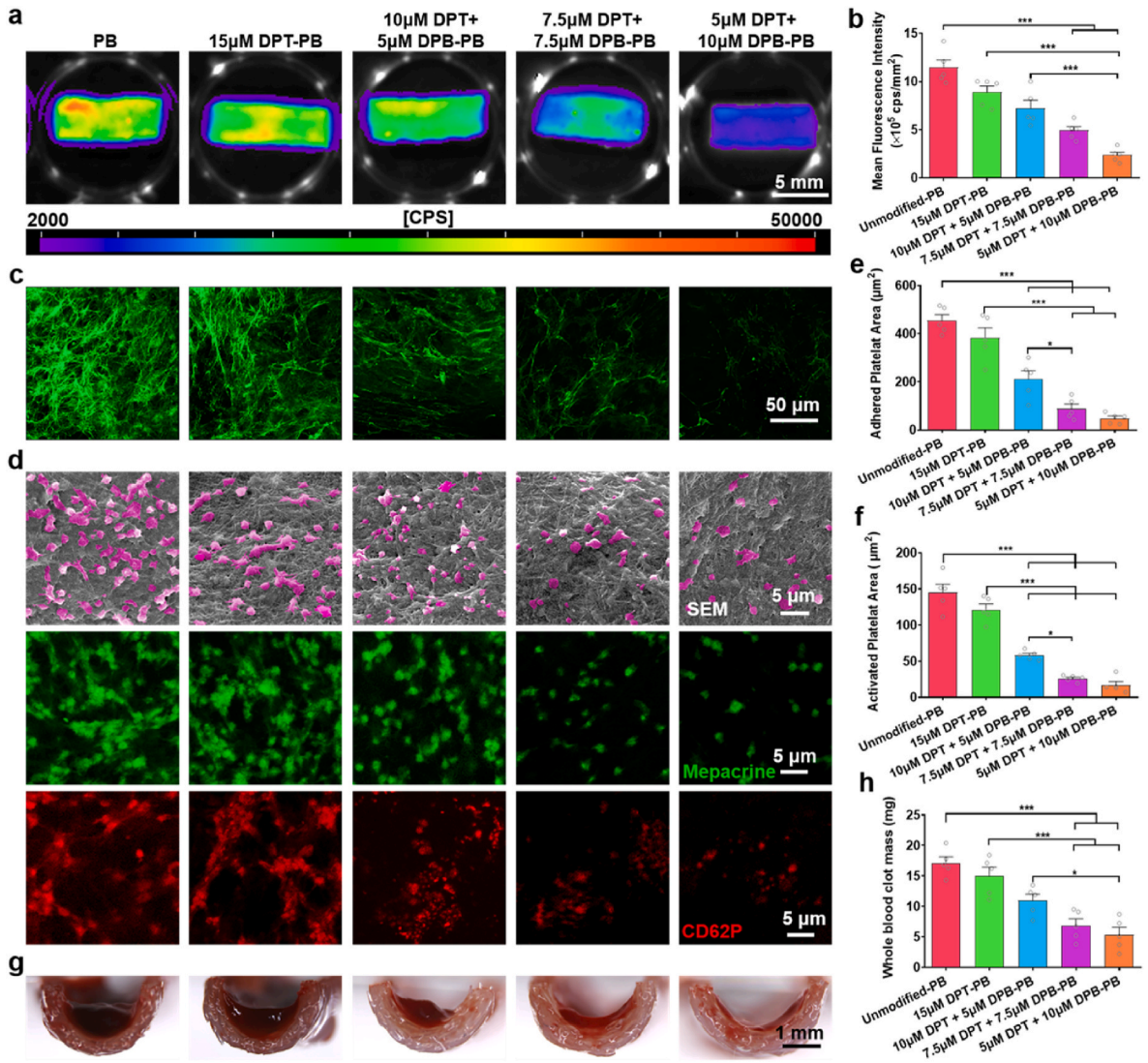

Fig. 3. Hemocompatibility analysis of differentially modified PBs. a) Representative fluorescence images and b) quantitative MFI analysis of Alexa Fluor 488-labelled FIB adhesion on the lumen surface of PBs with different modification treatment. c) Representative confocal images of fibrin network formed by adhered FIB on the lumen surface of PBs with differential modifications. d) After 1 h incubation at 37 °C, the adhesion of platelets to the lumen of differentially modified PBs was observed by SEM (top row) and mepacrine staining (middle row) and the activation of platelets on different sample was observed by anti-CD62P staining (bottom row). e,f) Quantitative analysis of e) the area occupied by adhered platelets and f) the area occupied by activated platelets per field of view, based on mepacrine staining and anti-CD62P staining images, respectively. Five image per samples and five samples per group were evaluated to obtain statistical results. g,h) After incubation at room temperature for 5 min, g) the clot of recalcified whole blood on the lumen of PBs with different modification was observed by a stereomicroscopic and h) quantified by weighting. Quantitative data are displayed as the mean ± SEM (n = 5). Statistical significance is indicated as $^{*}P < 0.05$, $^{***}P < 0.001$, ns = not significant. *P* values were determined using one-way ANOVA with Tukey's post hoc analysis.

thrombin's role as an agonist of platelet adhesion and activation [78]. Furthermore, we used recalcified whole blood to evaluation the anti-clot formation ability of differentially modified PBs. Stereomicroscopic observation revealed no obvious signs of blood clot formation on modified PBs when DPB concentrations exceeded 5 μM (Fig. 3g), and the inhibitory effect was further shown by the reduced clot mass (Fig. 3h). A series of works by previously, Yang et al. [75,79,80] showed that the surface of a BVLD-modified blood-interfacing material exhibited marked resistance to fibrin binding and platelet adhesion and activation, thereby effectively prevented thrombus formation. The above results support the incorporation of DPB modifications to effectively improve the hemocompatibility of PB lumens. Moreover, the data demonstrated that BVLD maintained its anticoagulation bioactivity despite conjugation with DMPE-PEG.

2.4. Protection of the specific capture of EPCs by DPB/DPT co-modifications

In addition to anti-coagulation modifications, pro-endothelialization modifications have been shown to be beneficial in achieving and maintaining TEVG patency [81]. Despite demonstratable success *in vitro* through enhanced adhesion and migration of ECs [28,82,83], the rapid adhesion of blood components to the blood-interfacing material surface *in vivo* could mask pro-endothelialization bioactive molecule, ultimately leading to invalidity of pro-endothelialization functional modifications [33]. Therefore, many research groups have co-modified PEG to protect the function of pro-endothelialization modifications, such as EPC-capturing ligands [11,84,85]. Despite PEG-modified implants supporting reduced adherence of non-specific blood proteins, PEG did not convey significant improvement of antithrombotic ability *in vivo* [86]. This may be explained by PEG lacking specific anticoagulant biological

effect [87]. The use of other anticoagulant molecules such as heparin, have been combined with bioactive molecules to promote endothelialization [88]. The anticoagulant ability of heparin is dependent on its capacity to bind circulating antithrombin [37]. However, heparin also binds plasma proteins such as growth factors and fibronectin [89]. Such non-specific interactions impact on the anticoagulant capabilities of heparin [43], which also does not resolve the issues relating to masking of functional co-modified molecules by blood components. Bovine serum albumin (BSA) is a commonly used model protein in the evaluation of the non-specific protein adsorption of materials [90,91]. There was no obvious differences in the amount of BSA adhered to the lumen of DPT-modified PBs, DPB-modified PBs, or DMPE-PEG (DP)-modified PBs, but all showed obviously lower BSA adherence than unmodified-PBs (Fig. S6, Supporting Information). These results suggested that the protection against non-specific protein adsorption function of the PEG components in DPT and DPB modifications was maintained. Thus, our data suggest that modification with PEG-BVLD is an effective method to provide anticoagulation whilst reducing nonspecific protein binding.

We next sought to determine whether DPB could prevent DPT from having its EPC-recruiting function masked by blood components. TPS peptide was conjugated with propargylglycine (PraOH) to synthesize DPT with an alkynyl end (DPT-PraOH) (Fig. S7, Supporting Information). DPT-PraOH modified PB lumens were reacted with Cy5-N_3 in the presence or absence of various concentrations of DPB. The capacity of DPB to repel blood components and to thereby allow Cy5-N_3 to react with available DPT-PraOH via click chemistry was determined by fluorescent signal intensity (Fig. 4a). After incubation with PBS for 1 h, all the DPT-PraOH modified on the lumen surface of PBs could react with Cy5-N_3 because there was no blood component adhesion to shield the DPT-PraOH molecules (Fig. 4b). Thus, the fluorescence intensity of Cy5 was positive correlation with DPT-PraOH modification concentration. Platelet-rich plasma (PRP) contains enriched blood plasma components, such as numerous platelets, plasma proteins, and near physiological levels of FIB [92,93]. Quantitative analysis (Fig. 4c) showed that after incubation with PRP, addition of Cy5-N_3 resulted in fluorescence signal that increased with the concentration increase of DPB modifications, which indicated that DPB successfully inhibited PRP-component adhesion and protected DPT-PraOH reaction with Cy5-N_3. The fluorescence intensity of the 7.5 μM DPT +7.5 μM DPB-PBs and 5 μM DPT +10 μM DPB-PBs groups showed no significant differences between PBS and PRP incubations, which revealed that the potent effect of ≥7.5 μM DPB on preventing DPT from PRP-component masking. Therefore, 7.5 μM DPT +7.5 μM DPB-PBs and 5 μM DPT +10 μM DPB-PBs were selected as optimized PB modification candidates for further evaluation.

Circulating cell populations consist of multiple cell types. One of the most abundant cell types found in circulation are monocytes. To

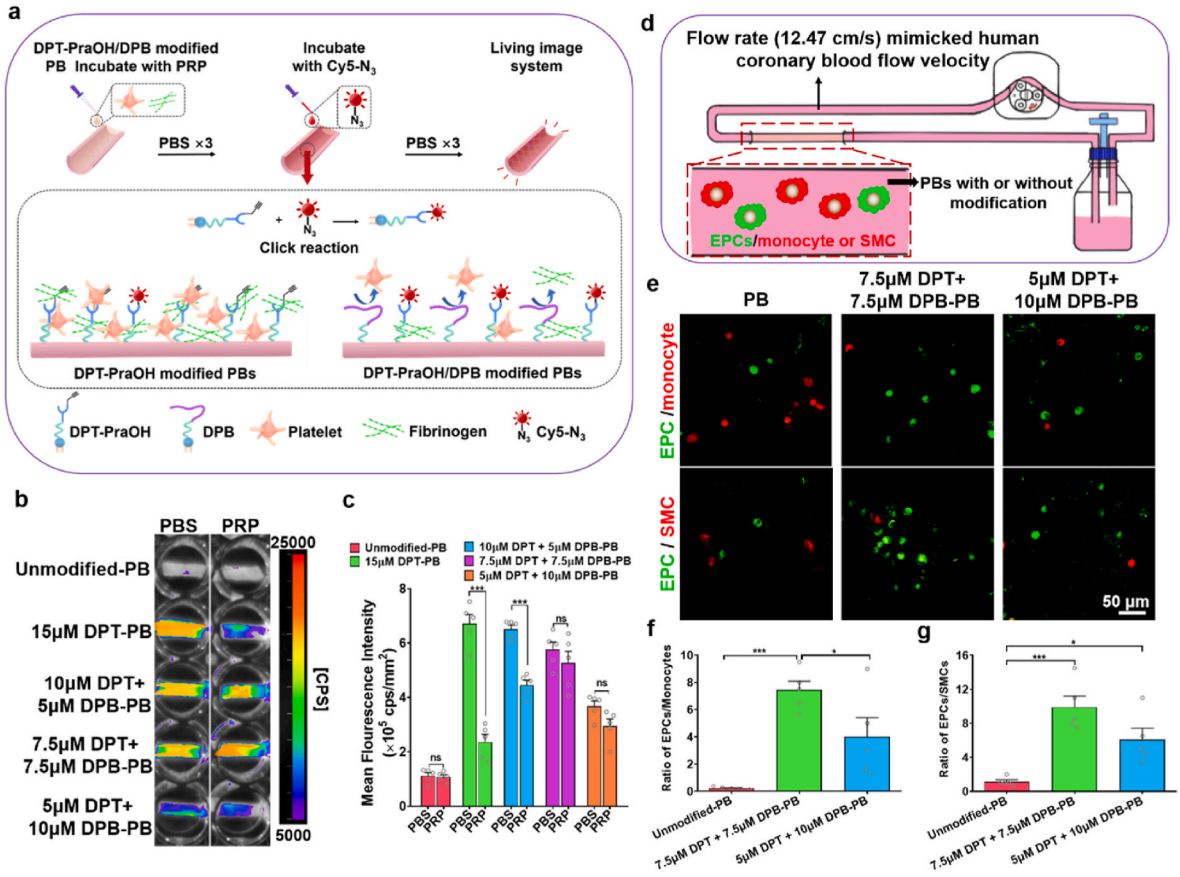

Fig. 4. Analysis of the protective effect of DPB on DPT and selective capture of EPCs by DPT modified PB lumens. a) A schematic showing the experimental design to evaluate DPB inhibition of DPT masking by blood components. b) The masking of DPT modified lumen surface of PBs was detected by Cy5 fluorescence imaging after incubation with PBS or PRP for 1 h. Stronger fluorescence signal represented that more DPT-PraOH was exposed to react with Cy5-N_3. c) Quantitative MFI analysis of Cy5 conjugated onto the lumen surface of PBs with different modification treatment in PBS and PRP group. Data are displayed as the mean ± SEM (n = 5). Statistical analysis is annotated as $^*P < 0.05$; $^{***}P < 0.001$; and ns (not significant), as determined using unpaired Student's *t*-tests. d) Schematic illustration of EPC selective capture experiments in dynamic flow culture system. e) Representative confocal images of DiO-labelled EPCs (green) and DiI-labelled monocyte (red) or DiI-labelled SMCs (red) adhesion on the lumen of different concentration of DPT: DPB modified PBs at 4 h post-dynamic flow culture. f,g) The adhesion ratios of f) EPCs/MNCs and g) EPCs/SMCs were calculated based on confocal images from e). Five image per sample and five samples per group were evaluated to obtain statistical results. Quantitative data are presented as the mean ± SEM (n = 5). Statistical analysis is annotated as $^*P < 0.05$; $^{***}P < 0.001$; and ns (not significant), as determined using one-way ANOVA with Tukey's post hoc analysis.

demonstrate selective EPC capture from a heterogeneous mixture of cells, 2×10^5 cells/mL DiO-labelled EPCs were mixed with 1×10^6 cells/mL DiI-labelled monocytes (1:5) and the cell mixture was then perfused over lumen surface of differentially modified PBs using a dynamic flow culture chamber (12.47 cm/s) over the course of 4 h. The flow rate of culture medium mimicked human coronary blood flow velocity (9.9 ± 3.5 cm/s) [64]. Confocal images (Fig. 4e) showed that compared to unmodified PBs, EPC capture and adhesion increased, whereas non-specific MNC adhesion was markedly reduced on the lumen surface of 7.5 μM DPT +7.5 μM DPB-PBs and 5 μM DPT +10 μM DPB-PBs.. Quantitatively, the adhered cell ratio of EPC: MNC (0.23 ± 0.09) on the lumen surface of unmodified PBs was comparable with the ratio of the initial 1:5 ratio of EPC: MNC in the mixed cell suspension, which indicated that the unmodified PBs lacked selectivity for cells adhesion. However, the EPC:MNC ratio demonstrated a substantial increase in the DPT/DPB modified PBs, and the highest ratio was found to be in the 7.5 μM DPT +7.5 μM DPB-PB group (Fig. 4f). In addition to the cells in circulation, balanced control over VSMCs infiltration is an important factor influencing physiological versus pathological vascular tissue regeneration [94,95]. The competitive growth of VSMCs can obstruct EC monolayer formation, resulting in intimal hyperplasia and compromised vascular graft patency [25,96]. The adhesion of EPCs and VSMCs exhibited a similar pattern to the previously observed EPCs and MNCs adhesion ratios (Fig. 4e,g), EPC:VSMC adhesion ratios were 1.13 ± 0.23, 9.90 ± 1.30, and 6.10 ± 1.32 on unmodified PBs, 7.5 μM DPT +7.5 μM DPB-PBs, and 5 μM DPT+ 10 μM DPB-PBs, respectively. These results indicated that the functional sites of DPT modified onto the lumen surface of PBs was effectively left exposed, due to the anti-making effect of co-modified DPB. The DPT modifications conveyed prominent EPC-capturing ability, thereby also demonstrating TPS functionality despite conjugation to DMPE-PEG.

2.5. *In vivo* endothelial regeneration by DPB/DPT-PBs in rat abdominal artery replacement models

The 7.5 μM DPT +7.5 μM DPB-PBs exhibited the optimal ability to selectively capture EPCs, but the complexity of the *in vivo* internal environment warranted the use of rat abdominal artery implantation to

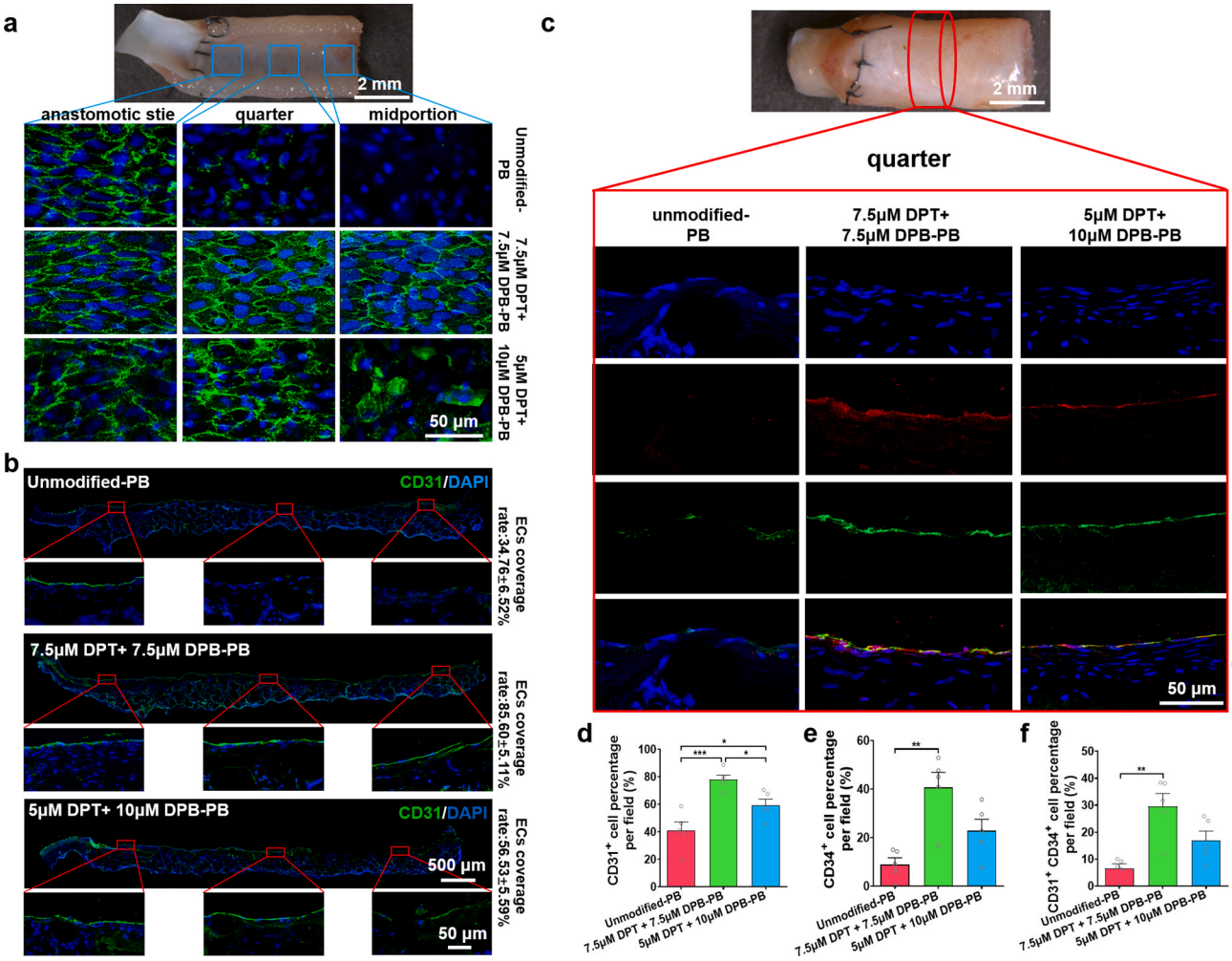

Fig. 5. Evaluation of ECs regeneration of DPT/DPB modified PBs after implantation into rat abdominal artery for 2 weeks. a) CD31 en-face staining showed the ECs coverage at different (anastomotic, quarter and midportion) sites of the lumen. b) Representative anti-CD31 antibody immunofluorescence staining images of longitudinal sections and calculated mean % ± SEM of ECs coverage (length of $CD31^+$ monolayer/total length) (n = 5). c) Representative double immunofluorescence staining images with anti-CD34 (red) and anti-CD31 (green) antibodies demonstrate the difference in the contribution of $CD34^+$ EPCs to the ECs regeneration at quarter site of the explanted PBs in different groups. Quantification of d) $CD31^+$ cells (% of total lumen-facing cells per field); e) $CD34^+$ cells (% of total lumen-facing cells per field); and f) $CD31^+$ $CD34^+$ double-positive cells (% of total lumen-facing cells per field). Quantification was assessed across the three assessed sites (anastomotic, quarter, midportion) of the lumen at 2 weeks post-implantation (1 images per sites, 3 different site per section, 3 section per sample and 5 samples per group were evaluated to obtain data for statistical analysis). Data are expressed as the mean ± SEM (n = 5). Statistical significance is indicated as $^*P < 0.05$, $^{***}P < 0.001$, ns = no significance. *P* values were determined using one-way ANOVA with Tukey's post hoc analysis.

assess the performance of both 7.5 μM DPT +7.5 μM DPB-PBs and 5 μM DPT +10 μM DPB-PBs. One week after vascular implantation, anti-CD34 and anti-Flk-1 antibodies were used to co-stain and characterize the presence of EPCs on the luminal surface of differentially modified PBs (Fig. S8, Supporting Information). On the lumen of unmodified PBs, $CD34^+$ Flk^+ cells were scarcely observable. In contrast, both 7.5 μM DPT +7.5 μM DPB-PBs and 5 μM DPT +10 μM-PBs exhibited more $CD34^+$ and Flk^+ cells on the lumen surfaces at all three of the assessed sites. The elevated luminal presence of cells positive for EPC markers indicated that DPT/DPB modified PBs successfully enhanced the capture of EPCs *in vivo*. After implantation for 2 weeks, en-face staining showed a different extent of EC coverage at the anastomotic site, quarter site and midportion site of the differentially modified PBs (Fig. 5a). In unmodified PBs, only the anastomotic sites showed EC coverage, likely indicative of *trans*-anastomotic migration of ECs rather than EPC recruitment [97]. In the 5 μM DPT +10 μM DPB-PB group, more ECs had covered the lumen surface, but complete EC monolayer regeneration had yet to be achieved, especially at the midportion site. In the 7.5 μM DPT +7.5 μM DPB-PBs group, the luminal surface at each of the three analysed sites had been completely covered by ECs with a morphology similar to native vascular tissue ECs (i.e., cobblestone-like morphology and elongated follow the blood flow direction) [98]. The same degree of coverage was also observed by immunofluorescence staining of the longitudinal sections using anti-CD31 antibody (Fig. 5b). The ECs coverage rates of 7.5 μM DPT +7.5 μM DPB-PBs was found to be 85.60 ± 5.11% at 2-week post-vascular implantation, which was a remarkably higher percentage than unmodified (34.76 ± 6.52%) and 5 μM DPT + 10 μM DPB-PBs (56.53 ± 5.59%) (Fig. S9, Supporting Information). To investigate whether the improved endothelialization of modified PBs was directly related to the enhanced and selective capture of EPCs, anti-CD34 antibody (a typical marker expressed by EPCs) [99] and anti-CD31 antibody co-staining were performed to disclose the contribution of $CD34^+$ EPCs to $CD31^+$ EC monolayer regeneration in differentially modified PBs at 2 weeks. Few $CD34^+$ $CD31^+$ cells were observed at the anastomotic site of unmodified PBs (Fig. S10, Supporting Information), and neither $CD31^+$ cells nor $CD34^+$ cells were distributed at the quarter site (Fig. 5c) or midportion sites of unmodified PBs (Fig. S10, Supporting Information). Both 7.5 μM DPT +7.5 μM DPB-PBs and 5 μM DPT +10 μM-PBs exhibited more $CD31^+$ $CD34^+$ cells on the lumen surface at all three of the assessed sites (Fig. 5c, Fig. S10, Supporting Information). Quantitative analysis indicated that 7.5 μM DPT +7.5 μM DPB-PBs showed the highest percentage of $CD31^+$ (Fig. 5d) and $CD34^+$ cells (Fig. 5e). The ratio of $CD31^+CD34^+$cells among the three PB groups indicated that 7.5 μM DPT +7.5 μM DPB-PBs demonstrated the highest ratio (29.50 ± 4.84%), followed by 5 μM DPT + 10 μM DPB-PBs (16.90 ± 3.53%) (Fig. 5f). The current generally accepted *in situ* endothelialization mechanism of vascular grafts include endothelial ingrowth from *trans*-anastomotic migration and recruitment/adhesion of circulating progenitor cells [100]. Our results strongly support the capture of circulating EPCs as an effective method to promote timely endothelialization. Accumulated evidence also demonstrated that EPCs stimulated the proliferation of mature ECs [101] and inhibited their apoptosis through paracrine activity [102]. Both our en-face staining and anti-CD31 antibody-stained longitudinal sections showed that the extent of EC monolayer regeneration closer to the anastomotic site was more consistent than at the distal midportion site. Therefore, EPCs captured by DPT may also assist in the promotion of vascular resident EC migration and proliferation from anastomosis-adjacent sites.

2.6. Performance of DPT/DPB modified PBs in canine carotid artery implantation models without anticoagulant administration

Thrombus formation is considered a predominant reason of vascular graft failure [3]. Antiplatelet drugs, such as aspirin or clopidogrel, are commonly used in clinical settings to maintain implanted graft patency [103]. However, the administration of antiplatelet drugs is a double-edged sword, as indicated by the increased risk of adverse bleeding described in clinical research studies [8]. In our previous study, orally administered antiplatelet drugs were required to maintain PB patency in canine carotid artery implantation models [51]. In this study, we evaluated platelet function via optical aggregometry after canines received the same anticoagulant administration as in our previous study (po: 13 mg/kg aspirin and 3 mg/kg clopidogrel, qd) for 7 consecutive days. Optical aggregometry is considered to be the 'gold standard' method for detecting drug-induced platelet dysfunction [104,105]. Aggregometry assesses platelet function using agonists to activate platelets and measures platelet aggregation [106]. After anticoagulant administration for 7 consecutive days, there was an approximately five-fold decrease in the maximal platelet aggregation when arachidonic acid was used as the agonist in canine (from 80.75 ± 4.81% to 15.63 ± 3.67%) (Fig. 6a). Cuticle bleeding time (CBT) assay was performed to evaluate the influence of anticoagulant administration on increasing bleed risk. After the canine nail cuticle was severed, the number of blood drops in the subsequent 15 min was recorded (Fig. 6b) and converted to a CBT score (Table S3, Supporting Information). The CBT score (Fig. 6c) of canine received anticoagulant drugs for 7 consecutive days was 36.88 ± 5.97, which was remarkably higher than that before anticoagulant administration (6.75 ± 1.36). A standardized cut with controlled length (2 cm) and depth (0.2 cm) on canine hind limb was produced to observe the bleeding. Before anticoagulant administration, only minimal bleeding with spontaneous hemostasis at 3 min. However, after canine received anticoagulant drugs for 7 consecutive days, active bleeding and significant increased amount of blood were observed at 3 min of incision produced. These results indicated that consist anticoagulant administration obviously increase the bleeding risk, which even may be fatal [8, 37]. Avoiding the use of anticoagulant drugs would improve the life quality of patients and should be the development trend of TEVG [107]. In order to clear the influence of anticoagulant drug on the patency of vascular grafts, the canine received a 3-week wash out period without any drug administration [108]. Afterwards, the eight canine were randomly divided into two groups to evaluate the performance of the modified and unmodified PBs in carotid artery implantation model without any anticoagulant administration (Fig. 6e). After vascular implantation for 30 days, color ultrasound doppler test showed that the patency rate of 7.5 μM DPT +7.5 μM DPB-PBs was 75%, while all the unmodified PBs was occlusion (Fig. 6f and Fig. S11, Supporting Information). Color ultrasound doppler test also showed that compared to immediate test post-vascular implantation, there was only a slight decrease in luminal diameter of the patent 7.5 μM DPT +7.5 μM DPB-PBs at 30 days (Fig. 6g). Stereomicroscopic observation showed that there were lots of capillaries on the outer surface of the explanted unmodified PBs and 7.5 μM DPT +7.5 μM DPB-PB, indicating that co-modification had no influence on the integration of PBs with the surrounding tissue (Fig. 6h). Stereomicroscopy (Fig. 6h and Fig. S12, Supporting Information) images of the cross section from proximal anastomoses (position #1), midportion (position #2) and distal anastomoses (position #3) together with H&E staining (Fig. 6i) confirmed that the thrombus formation was the main cause of the occlusion in the all unmodified-PBs and 7.5 μM DPT +7.5 μM DPB-PBs. The lumen surface of the other three patent 7.5 μM DPT +7.5 μM DPB-PBs at midportion was free of thrombus (Fig. S12, Supporting Information). SEM images (Fig. 6j) showed that the lumen surface of patent 7.5 μM DPT +7.5 μM DPB-PBs has covered by cobblestone-like ECs with a nicely elongation in the direction of blood flow, similar to regenerated ECs in rat model. Immunofluorescence staining of vWF and α-SMA (Fig. 6k) showed that the lumen of patent 7.5 μM DPT +7.5 μM DPB-PBs were covered by vWF^+ EC monolayer, $\alpha\text{-SMA}^+$ SMCs were arranged in the circumferential direction and closely adhered blow the EC layer. These results indicated that 7.5 μM DPT +7.5 μM DPB-PB display the good capacity for rapid endothelialization and vascular regeneration.

Assessment of modification stability indicated the degree of loss of functional molecules from the lumen surface of PBs, which may result in

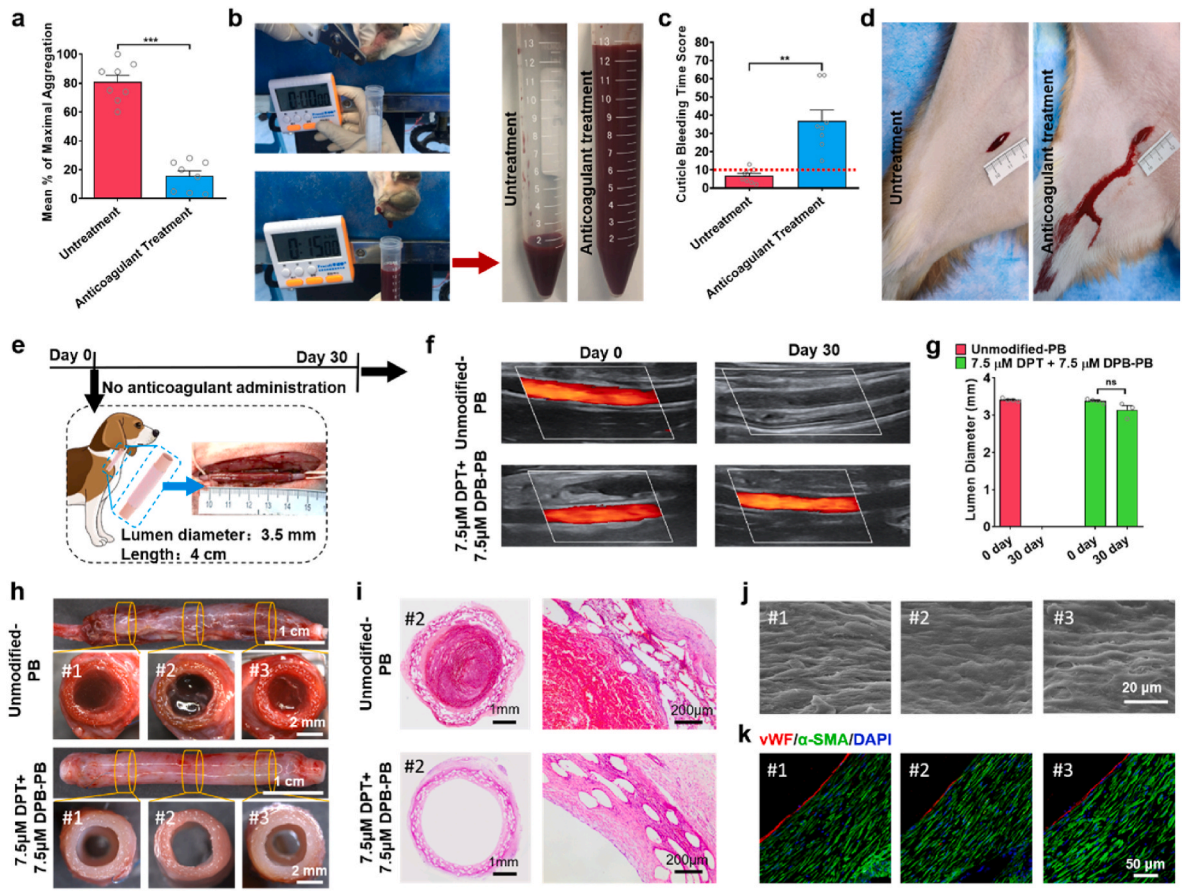

Fig. 6. Evaluation of the bleeding risk caused by anticoagulant administration and the performance of 7.5 μM DPT +7.5 μM DPB-PB in canine model. a-d) Evaluation of canine bleeding risk before and after anticoagulant administration (po: 13 mg/kg aspirin and 3 mg/kg clopidogrel, qd) for 7 consecutive days. a) Maximum platelet aggregation percentage analysis via optical aggregometry in eight dogs before anticoagulant administration and after 2 h at the last anticoagulant administration. b) Nail cuticle bleeding time (CBT) assay. After the nail cuticle was severed, the number of blood drops in the subsequent 15 min was recorded and converted to a CBT score (Table S3, Supporting Information). c) Statistical analysis of canine CBT scores before and after anticoagulant administration for 7 days (n = 8). d) Representative digital photos of full-thickness skin incision bleeding assay. e-k) Performance evaluation of modified and unmodified PBs in canine carotid artery implantation model. e) The 7.5 μM DPT +7.5 μM DPB-PBs and unmodified PBs were implantated into canine carotid artery for 30 days without any anticoagulant administration. f) Representative colour ultrasound doppler images of implanted graft immediately after surgery (day 0) and 30 days post-vascular implantation (day 30). g) Quantitative analysis of luminal diameter based on colour ultrasound doppler test (n = 4). h) Representative stereomicroscopy images of side view and cross-section of the explanted 7.5 μM DPT +7.5 μM DPB-PB and unmodified PBs at 30 days. i) Representative H&E staining images of the cross-section of midportion of the explanted 7.5 μM DPT +7.5 μM DPB-PB and unmodified-PBs. j, k) Representative j) lumen surface SEM images and k) anti-vWF immunofluorescence staining images of three different (proximal anastomoses, midportion and distal anastomoses) sites of the explanted 7.5 μM DPT + 7.5 μM DPB-PBs at 30 days. Data are shown as means ± SEM. Statistical significance was determined by paired Student's t-test (a, c, g). $^{**}P < 0.01$, $^{***}P < 0.001$ and ns: not significant.

systemic distribution of DPT and DPB with risks of adverse effects. Thus, the major organs were evaluated for signs of toxicity (heart, liver, spleen, lung, kidney). H&E staining showed that the histological architecture of main organs of rats from DPT/DPB modified PBs groups was similar to those from unmodified PBs at 2-week post-vascular implantation, which both had no abnormal pathological changes compared to those form normal rats without any treatment (Fig. S13, Supporting Information). In canine vascular implantation model, the abnormal pathological changes were not be found in main organs at 30 days (Fig. S14, Supporting Information). These results indicated that the loss of DPB and DPT modifications from the lumen surface did not induce organ toxicity.

The work presented here offers insights into the feasibility of achieving biocompatible and functional modifications in living cell systems. Indeed, this cell membrane modification method may have general applications in the field of tissue-engineered constructs containing living cells or for conveying beneficial function for organ transplantation. Vascularization is one of the top challenges in engineered tissues and organs [109]. Especially for large size (>1 mm) tissue constructs replacements, angiogenesis should be considered [110]. Bioactive molecules that promote angiogenesis and vascularization, such as IGF-mimicking peptide [111], could be modified onto the surface of transplanted allogeneic tissues or tissue-engineering constructs using anchors/linkers DMPE-PEG. A promising therapeutic method for type 1 diabetes is islet transplantation. However, host immune rejection as mediated by T effector cells severely limit the functions and longevity of grafted allogeneic islets [112]. Using DMPE-PEG covalent linked with immunomodulatory molecules to modify islet cell surfaces could potentially serve to help alleviate immune rejection. The present study can serve as a foundational basis and reference from which to adapt DMPE-PEG-molecule modifications into complex tissue/organ structures.

3. Conclusion

Through the conjugation of BVLD or TPS to DMPE-PEG, we successfully synthesized DPB and DPT, respectively. These two types of molecular modifications were co-modified onto the lumen surface of PBs, by utilizing hydrophobic interactions between DMPE-PEG and the living cell membranes. The biocompatible DPB and DPT co-

modifications afforded PBs the capacity to attenuate fibrinogen binding, platelet adhesion, and whole blood clot formation on the material-blood interface; whilst also facilitating the specific capture and recruitment of EPCs from the circulating blood to enhance endothelialization. A total of 10 min of incubation time was sufficient to saturate the PB lumens with DPB and DPT. The optimized DPT/DPB-PB could then be immediately implanted as vascular grafts to achieve remarkable improvements in patency and graft endothelialization in both small-animal (rat) and large-animal (canine) artery replacement models. Importantly, these beneficial effects were realised without the need for anticoagulant drug administration. The uniqueness of this work was summarized as follows: (i) Conjugation of BVLD or TPS to DMPE-PEG successfully produced synthetic DPB and DPT molecules. The two molecules were co-modified on the lumen surface of PBs, based on the hydrophobic interactions between DMPE-PEG and cell membranes. DMPE-PEG-based functional modifications exhibited high efficiency and biocompatibility, achieving saturated levels of modification within 10 min of incubation, which did not exert negative impacts on PB-resident cell viability or expression of physiological markers (apoptosis and metabolism-related gene expression); (ii) DPB modifications achieved an effective 'kill three birds with one stone' strategy. The DPB modifications conveyed anti-coagulation functions and maintained the nonspecific protein repellent function of its PEG component, which in-turn prevented DPT from having its EPC-recruiting function masked by circulating blood components; (iii) DPT and DPB co-modified PBs maintained vascular graft patency and facilitated the rapid endothelialization of grafts implanted in large animal carotid artery replacement models without the requirement for administration of anticoagulation drugs; and (iv)This work provided a safe, simple and fast approach to modify tissue engineering constructs containing live cells.

Ethics approval and consent to participate

- All animal studies were performed according to the guidelines set by the Tianjin Committee of Use and Care of Laboratory Animals, and the overall project protocols were approved by the Animal Ethics Committee of Nankai University. The accreditation number of the laboratory is SYXK (Jin) 2019–0003 promulgated by the Tianjin Science and Technology Commission.
- All studies using human peripheral blood were approved by Nankai University Institutional Review Board (approval number NKUIRB2022048).

CRediT authorship contribution statement

Hongyu Yan: Conceptualization, Data curation, Formal analysis, Investigation, Methodology, Visualization, Writing – original draft, Writing – review & editing. **Quhan Cheng:** Data curation, Formal analysis, Investigation, Visualization, Writing – original draft, Writing – review & editing. **Jianghua Si:** Validation, Investigation. **Songdi Wang:** Validation, Investigation. **Ye Wan:** Investigation. **Xin Kong:** Investigation. **Ting Wang:** Writing – original draft, Writing – review & editing. **Wenting Zheng:** Resources, Methodology. **Muhammad Rafique:** Investigation. **Xiaofeng Li:** Resources, Software. **Ju He:** Resources, Methodology. **Adam C. Midgley:** Supervision, Funding acquisition, Project administration, Writing – original draft, Writing – review & editing. **Yi Zhu:** Writing – original draft, Writing – review & editing. **Kai Wang:** Conceptualization, Supervision, Methodology, Funding acquisition, Project administration, Writing – original draft, Writing – review & editing. **Deling Kong:** Supervision, Funding acquisition, Project administration, Writing – original draft, Writing – review & editing.

Declaration of competing interest

The authors have no conflicts of interest to disclose in relation to this article.

Acknowledgements

All animal studies were performed according to the guidelines set by the Tianjin Committee of Use and Care of Laboratory Animals, and the overall project protocols were approved by the Animal Ethics Committee of Nankai University. The accreditation number of the laboratory is SYXK (Jin) 2019–0003 promulgated by the Tianjin Science and Technology Commission. We thank D. Zhi, T. Yang, and J. Zhang for technical assistance and helpful discussions. Funding: This work was supported by the National Natural Science Foundation of China (NSFC) projects 81921004 (D. K.), 82127808 (D. K.), 32222043 (K.W.), 82250610231 (A. C. M.), National Key R&D Program of China 2022YFA1105102 (K.W.), Tianjin Natural Science Foundation 20JCYBJC01150 (K.W.), Tianjin Natural Science Foundation 18JCZDJC37600 (K.W.), NCC Fund NCC2020PY18 (K.W.), and Tianjin "Project + Team" Key Training Foundation XC202035 (K.W.). **Competing interests:** The authors declare that they have no competing interests. **Data and materials availability:** All data needed to evaluate the conclusions in the paper are present in the paper and/or the Supplementary Materials.

Appendix A. Supplementary data

Supplementary data to this article can be found online at https://doi.org/10.1016/j.bioactmat.2023.03.003.

References

[1] L.E. Niklason, J.H. Lawson, Bioengineered human blood vessels, Science 370 (6513) (2020), eaaw8682.
[2] A. Fayon, P. Menu, R. El Omar, Cellularized small-caliber tissue-engineered vascular grafts: looking for the ultimate gold standard, Npj Regenerative Medicine 6 (1) (2021) 1–11.
[3] P. Gupta, B.B. Mandal, Tissue-engineered vascular grafts: emerging trends and technologies, Adv. Funct. Mater. 31 (33) (2021), 2100027.
[4] S. Dimitrievska, J. Wang, T. Lin, A. Weyers, H. Bai, L. Qin, G. Li, C. Cai, A. Kypson, N. Kristofik, A. Gard, S. Sundaram, K. Yamamoto, W. Wu, L. Zhao, M. H. Kural, Y. Yuan, J. Madri, T.R. Kyriakides, R.J. Linhardt, L.E. Niklason, Glycocalyx-like hydrogel coatings for small diameter vascular grafts, Adv. Funct. Mater. 30 (23) (2020), 1908963.
[5] M. Gorbet, C. Sperling, M.F. Maitz, C.A. Siedlecki, C. Werner, M.V. Sefton, The blood compatibility challenge. Part 3: material associated activation of blood cascades and cells, Acta Biomater. 94 (2019) 25–32.
[6] D. Radke, W. Jia, D. Sharma, K. Fena, G. Wang, J. Goldman, F. Zhao, Tissue engineering at the blood-contacting surface: a review of challenges and strategies in vascular graft development, Adv. Healthc. Mater. 7 (15) (2018), 1701461.
[7] K. Solo, S. Lavi, C. Kabali, G.N. Levine, A. Kulik, A.A. John-Baptiste, S.E. Fremes, J. Martin, J.W. Eikelboom, M. Ruel, A.A. Huitema, T. Choudhury, D.L. Bhatt, N. Tzemos, A.M. Mamas, R. Bagur, Antithrombotic treatment after coronary artery bypass graft surgery: systematic review and network meta-analysis, Br. Med. J. 367 (2019), 15476.
[8] C. Sostres, B. Marcen, V. Laredo, E. Alfaro, L. Ruiz, P. Camo, P. Carrera-Lasfuentes, A. Lanas, Risk of rebleeding, vascular events and death after gastrointestinal bleeding in anticoagulant and/or antiplatelet users, Aliment, Pharmacol. Ther. 50 (8) (2019) 919–929.
[9] W. Peng, P. Liu, X. Zhang, J. Peng, Y. Gu, X. Dong, Z. Ma, P. Liu, J. Shen, Multi-functional zwitterionic coating for silicone-based biomedical devices, Chem. Eng. J. 398 (2020), 125663.
[10] J. Zhang, L. He, G. Wei, X. Jiang, L. Fu, Y. Zhao, L. Zhang, L. Yang, Y. Li, Y. Wang, H. Mo, J. Shen, Zwitterionic oolymer-grafted polylactic acid vascular patches based on a decellularized scaffold for tissue engineering, ACS Biomater. Sci. Eng. 5 (9) (2019) 4366–4375.
[11] Q. Ji, S. Zhang, J. Zhang, Z. Wang, J. Wang, Y. Cui, L. Pang, S. Wang, D. Kong, Q. Zhao, Dual functionalization of poly(epsilon-caprolactone) film surface through supramolecular assembly with the aim of promoting in situ endothelial progenitor cell attachment on vascular grafts, Biomacromolecules 14 (11) (2013) 4099–4107.
[12] Q. Zhang, C.R. Wang, Y. Babukutty, T. Ohyama, M. Kogoma, M. Kodama, Biocompatibility evaluation of ePTFE membrane modified with PEG in atmospheric pressure glow discharge, J. Biomed. Mater. Res. 60 (3) (2002) 502–509.
[13] R. Khalifehzadeh, W. Ciridon, B.D. Ratner, Surface fluorination of polylactide as a path to improve platelet associated hemocompatibility, Acta Biomater. 78 (2018) 23–35.
[14] M. Paven, P. Papadopoulos, S. Schoettler, X. Deng, V. Mailaender, D. Vollmer, H.-J. Butt, Super liquid-repellent gas membranes for carbon dioxide capture and heart-lung machines, Nat. Commun. 4 (2013) 2512.

[15] I.H. Jaffer, J.C. Fredenburgh, J. Hirsh, J.I. Weitz, Medical device-induced thrombosis: what causes it and how can we prevent it? J. Thromb. Haemostasis 13 (2015) S72–S81.
[16] S.A. Irvine, X. Yun, S. Venkatraman, Anti-platelet and tissue engineering approaches to biomaterial blood compatibilization: how well have these been translated into the clinic? Drug Deliv. Transl. Res. 2 (5) (2012) 384–397.
[17] Y. Wang, B. Ma, K. Liu, R. Luo, Y. Wang, A multi-in-one strategy with glucose-triggered long-term antithrombogenicity and sequentially enhanced endothelialization for biological valve leaflets, Biomaterials 275 (2021), 120981.
[18] Y. Yang, P. Gao, J. Wang, Q. Tu, L. Bai, K. Xiong, H. Qiu, X. Zhao, M.F. Maitz, H. Wang, X. Li, Q. Zhao, Y. Xiao, N. Huang, Z. Yang, Endothelium-mimicking multifunctional coating modified cardiovascular stents via a stepwise metal-catechol-(amine) surface engineering strategy, Research (2020) 2020.
[19] D.E. Heath, Promoting endothelialization of polymeric cardiovascular biomaterials, Macromol. Chem. Phys. 218 (8) (2017), 1600574.
[20] J.C. Deng, S.H. Yuan, X. Li, K.B. Wang, L.X. Xie, N. Li, J. Wang, N. Huang, Heparin/DNA aptamer co-assembled multifunctional catecholamine coating for EPC capture and improved hemocompatibility of vascular devices, Mat Sci Eng C-Mater. 79 (2017) 305–314.
[21] Y.Y. Duan, S. Yu, P.F. Xu, X.M. Wang, X. Feng, Z.W. Mao, C.Y. Gao, Co-immobilization of CD133 antibodies, vascular endothelial growth factors, and REDV peptide promotes capture, proliferation, and differentiation of endothelial progenitor cells, Acta Biomater. 96 (2019) 137–148.
[22] F. Kou, C. Zhu, H.J. Wan, F.L. Xue, J.F. Wang, L.J. Xiang, J.A. Li, Endothelial progenitor cells as the target for cardiovascular disease prediction, personalized prevention, and treatments: progressing beyond the state-of-the-art, EPMA J. 11 (4) (2020) 629–643.
[23] J.H. Collier, T. Segura, Evolving the use of peptides as components of biomaterials, Biomaterials 32 (18) (2011) 4198–4204.
[24] L.M. Wei, X.Y. Wang, C. Li, X.X. Li, Y.M. Yin, G.X. Li, Colorimetric assay for protein detection based on "nano-pumpkin" induced aggregation of peptide-decorated gold nanoparticles, Biosens. Bioelectron. 71 (2015) 348–352.
[25] Z.L. Yang, X. Zhao, R. Hao, Q.F. Tu, X.H. Tian, Y. Xiao, K.Q. Xiong, M. Wang, Y. H. Feng, N. Huang, G.Q. Pan, Bioclickable and mussel adhesive peptide mimics for engineering vascular stent surfaces, Proc. Natl. Acad. Sci. USA 117 (28) (2020) 16127–16137.
[26] H.Q. Chen, X.J. Li, Y.C. Zhao, J.A. Li, J. Chen, P. Yang, M.F. Maitz, N. Huang, Construction of a multifunctional coating consisting of phospholipids and endothelial progenitor cell-specific peptides on titanium substrates, Appl. Surf. Sci. 347 (2015) 169–177.
[27] H.Q. Chen, Y.C. Zhao, K.Q. Xiong, J.G. Li, J. Chen, P. Yang, N. Huang, Multifunctional coating based on EPC-specific peptide and phospholipid polymers for potential applications in cardiovascular implants fate, J. Mater. Chem.B 4 (48) (2016) 7870–7881.
[28] Z.Y. Chen, Q.L. Li, J.L. Chen, R.F. Luo, M.F. Maitz, N. Huang, Immobilization of serum albumin and peptide aptamer for EPC on polydopamine coated titanium surface for enhanced in-situ self-endothelialization, Mat Sci Eng C-Mater. 60 (2016) 219–229.
[29] Q. Li, Z. Wang, S. Zhang, W. Zheng, Q. Zhao, J. Zhang, L. Wang, S. Wang, D. Kong, Functionalization of the surface of electrospun poly(epsilon-caprolactone) mats using zwitterionic poly(carboxybetaine methacrylate) and cell-specific peptide for endothelial progenitor cells capture, Mat Sci Eng C-Mater. 33 (3) (2013) 1646–1653.
[30] M.C. Munisso, T. Yamaoka, Novel peptides for small-caliber graft functionalization selected by a phage display of endothelial-positive/platelet-negative combined selection, J. Mater. Chem. B 5 (47) (2017) 9354–9364.
[31] J. Fang, J.L. Zhang, J. Du, Y.J. Pan, J. Shi, Y.X. Peng, W.M. Chen, L. Yuan, S. H. Ye, W.R. Wagner, M. Yin, X.M. Mo, Orthogonally functionalizable polyurethane with subsequent modification with heparin and endothelium-inducing peptide aiming for vascular reconstruction, ACS Appl. Mater. 8 (23) (2016) 14442–14452.
[32] A.N. Veleva, D.E. Heath, S.L. Cooper, C. Patterson, Selective endothelial cell attachment to peptide-modified terpolymers, Biomaterials 29 (27) (2008) 3656–3661.
[33] J.H. Pang, Y. Farhatnia, F. Godarzi, A. Tan, J. Rajadas, B.G. Cousins, A. M. Seifalian, In situ endothelialization: bioengineering considerations to translation, Small 11 (47) (2015) 6248–6264.
[34] X. Ren, Y. Feng, J. Guo, H. Wang, Q. Li, J. Yang, X. Hao, J. Lv, N. Ma, W. Li, Surface modification and endothelialization of biomaterials as potential scaffolds for vascular tissue engineering applications, Chem. Soc. Rev. 44 (15) (2015) 5680–5742.
[35] Q. Li, Z.H. Wang, S.A. Zhang, W.T. Zheng, Q. Zhao, J. Zhang, L.Y. Wang, S. F. Wang, D.L. Kong, Functionalization of the surface of electrospun poly(epsilon-caprolactone) mats using zwitterionic poly(carboxybetaine methacrylate) and cell-specific peptide for endothelial progenitor cells capture, Mat Sci Eng C-Mater. 33 (3) (2013) 1646–1653.
[36] M. Avci-Adali, H. Stoll, N. Wilhelm, N. Perle, C. Schlensak, H.P. Wendel, In vivo tissue engineering: mimicry of homing factors for self-endothelialization of blood-contacting materials, Pathobiology 80 (4) (2013) 176–181.
[37] M. Badv, F. Bayat, J.I. Weitz, T.F. Didar, Single and multi-functional coating strategies for enhancing the biocompatibility and tissue integration of blood-contacting medical implants, Biomaterials 258 (2020), 120291.
[38] R.S. Navarro, L.T. Jiang, Y. Ouyang, J.W. Luo, Z.Y. Liu, Y. Yang, P. Qiu, K. Kuroda, Y.E. Chen, P.X. Ma, B. Yang, Biomimetic tubular scaffold with heparin conjugation for rapid degradation in in situ regeneration of a small diameter neoartery, Biomaterials 274 (2021), 120874.
[39] S. Dimitrievska, C. Cai, A. Weyers, J.L. Balestrini, T. Lin, S. Sundaram, G. Hatachi, D.A. Spiegel, T.R. Kyriakides, J.J. Miao, G.Y. Li, L.E. Niklason, R.J. Linhardt, Click-coated, heparinized, decellularized vascular grafts, Acta Biomater. 13 (2015) 177–187.
[40] C.J. Lee, J.E. Ansell, Direct thrombin inhibitors, Br. J. Clin. Pharmacol. 72 (4) (2011) 581–592.
[41] S. Pacelli, V. Manoharan, A. Desalvo, N. Lomis, K.S. Jodha, S. Prakash, A. Paul, Tailoring biomaterial surface properties to modulate host-implant interactions: implication in cardiovascular and bone therapy, J. Mater. Chem. B 4 (9) (2016) 1586–1599.
[42] D.T. Eitzman, L. Chi, L. Saggin, R.S. Schwartz, B.R. Lucchesi, W.P. Fay, Heparin neutralization by platelet-rich thrombi. Role of platelet factor 4, Circulation 89 (4) (1994) 1523–1529.
[43] C.J. Van Delden, G.H.M. Engbers, J. Feijen, The effect of protein adsorption on the anticoagulant activity of surface immobilized heparin, J. Biomater. Sci. Polym. Ed. 7 (8) (1996) 727–740.
[44] M. Ashcraft, M. Douglass, Y. Chen, H. Handa, Combination strategies for antithrombotic biomaterials: an emerging trend towards hemocompatibility, Biomater. Sci. 9 (7) (2021) 2413–2423.
[45] J.B. Larsen, A.-M. Hvas, Thrombin: a pivotal player in hemostasis and beyond, Semin, Thromb. Hemost 47 (2021) 759–774, 07.
[46] M.S. Lee, R.R. Makkar, Bivalirudin in acute coronary syndrome's and percutaneous coronary intervention, Rev. Cardiovasc. Med. 7 (2006) S27–S34.
[47] R.K. Ramana, B.E. Lewis, Percutaneous coronary intervention in patients with acute coronary syndrome: focus on bivalirudin, Vasc, Healthc. Risk Manag. 4 (3) (2008) 493–505.
[48] M.D. Moen, G.M. Keating, K. Wellington, Bivalirudin - a review of its use in patients undergoing percutaneous coronary intervention, Drugs 65 (13) (2005) 1869–1891.
[49] M. Yamanami, Y. Yahata, M. Uechi, M. Fujiwara, H. Ishibashi-Ueda, K. Kanda, T. Watanabe, T. Tajikawa, K. Ohba, H. Yaku, Y. Nakayama, Development of a completely autologous valved conduit with the sinus of Valsalva using in-body tissue architecture technology: a pilot study in pulmonary valve replacement in a beagle model, Circulation 122 (11 Suppl) (2010) S100–S106.
[50] W.J. Geelhoed, L. Moroni, J.I. Rotmans, Utilizing the foreign body response to grow tissue engineered blood vessels in vivo, J. Cardiovasc. Transl. Res. 10 (2) (2017) 167–179.
[51] D. Zhi, Q. Cheng, A.C. Midgley, Q. Zhang, T. Wei, Y. Li, T. Wang, T. Ma, M. Rafique, S. Xia, Y. Cao, Y. Li, J. Li, Y. Che, M. Zhu, K. Wang, D. Kong, Mechanically reinforced biotubes for arterial replacement and arteriovenous grafting inspired by architectural engineering, Sci. Adv. 8 (11) (2022), eabl3888.
[52] T.C. Rothuizen, F.F.R. Damanik, T. Lavrijsen, M.J.T. Visser, J.F. Hamming, R. A. Lalai, J.M.G.J. Duijs, A.J. van Zonneveld, I.E. Hoefer, C.A. van Blitterswijk, T. J. Rabelink, L. Moroni, J.I. Rotmans, Development and evaluation of in vivo tissue engineered blood vessels in a porcine model, Biomaterials 75 (2016) 82–90.
[53] Y. Teramura, H. Iwata, Cell surface modification with polymers for biomedical studies, Soft Matter 6 (6) (2010) 1081–1091.
[54] H. Yan, X. Mi, A.C. Midgley, X. Du, Z. Huang, T. Wei, R. Liu, T. Ma, D. Zhi, D. Zhu, T. Wang, G. Feng, Y. Zhao, W. Zhang, J. He, M. Zhu, D. Kong, K. Wang, Targeted repair of vascular injury by adipose-derived stem cells modified with P-selectin binding peptide, Adv. Sci. 7 (11) (2020), 1903516.
[55] W.J. Geelhoed, L. Moroni, J.I. Rotmans, Utilizing the foreign body response to grow tissue engineered blood vessels in vivo, J. Cardiovasc. Transl. 10 (2) (2017) 167–179.
[56] Y. Nakayama, M. Furukoshi, T. Terazawa, R. Iwai, Development of long in vivo tissue-engineered "Biotube" vascular grafts, Biomaterials 185 (2018) 232–239.
[57] K.M. Elson, N. Fox, J.L. Tipper, J. Kirkham, R.M. Hall, J. Fisher, E. Ingham, Non-destructive monitoring of viability in an ex vivo organ culture model of osteochondral tissue, Eur. Cell. Mater. 29 (2015) 356–369.
[58] J. Park, B. Andrade, Y. Seo, M.-J. Kim, S.C. Zimmerman, H. Kong, Engineering the surface of therapeutic "living" cells, Chem. Rev. 118 (4) (2018) 1664–1690.
[59] S. De Koker, B.G. De Geest, C. Cuvelier, L. Ferdinande, W. Deckers, W.E. Hennink, S. De Smedt, N. Mertens, Vivo cellular uptake, degradation, and biocompatibility of polyelectrolyte microcapsules, Adv. Funct. Mater. 17 (18) (2007) 3754–3763.
[60] S.-Y. Zhang, Z.-R. Zhou, R.-C. Qian, Recent progress and perspectives on cell surface modification, Chem. Asian J. 16 (21) (2021) 3250–3258.
[61] H. Cheng, M. Byrska-Bishop, C.T. Zhang, C.J. Kastrup, N.S. Hwang, A.K. Tai, W. W. Lee, X. Xu, M. Nahrendorf, R. Langer, D.G. Anderson, Stem cell membrane engineering for cell rolling using peptide conjugation and tuning of cell-selectin interaction kinetics, Biomaterials 33 (20) (2012) 5004–5012.
[62] M. Manrique-Moreno, M. Suwalsky, F. Villena, P. Garidel, Effects of the nonsteroidal anti-inflammatory drug naproxen on human erythrocytes and on cell membrane molecular models, Biophys. Chem. 147 (1–2) (2010) 53–58.
[63] K. Tatsumi, K. Ohashi, Y. Teramura, R. Utoh, K. Kanegae, N. Watanabe, S. Mukobata, M. Nakayama, H. Iwata, T. Okano, The non-invasive cell surface modification of hepatocytes with PEG-lipid derivatives, Biomaterials 33 (3) (2012) 821–828.
[64] R.R. Edelman, W.J. Manning, E. Gervino, W. Li, Flow velocity quantification in human coronary arteries with fast, breath-hold MR angiography, JMRI 3 (5) (1993) 699–703.
[65] Y. Teramura, H. Iwata, Improvement of graft survival by surface modification with poly(ethylene glycol)-lipid and urokinase in intraportal islet transplantation, Transplantation 91 (3) (2011) 271–278.

[66] S. Miura, Y. Teramura, H. Iwata, Encapsulation of islets with ultra-thin polyion complex membrane through poly(ethylene glycol)-phospholipids anchored to cell membrane, Biomaterials 27 (34) (2006) 5828–5835.
[67] D.C. Leslie, A. Waterhouse, J.B. Berthet, T.M. Valentin, A.L. Watters, A. Jain, P. Kim, B.D. Hatton, A. Nedder, K. Donovan, E.H. Super, C. Howell, C.P. Johnson, T.L. Vu, D.E. Bolgen, S. Rifai, A.R. Hansen, M. Aizenberg, M. Super, J. Aizenberg, D.E. Ingber, A bioinspired omniphobic surface coating on medical devices prevents thrombosis and biofouling, Nat. Biotechnol. 32 (11) (2014) 1134–1140.
[68] E.V. Lugovskoy, P.G. Gritsenko, T.A. Koshel, I.O. Koliesnik, S.O. Cherenok, O. I. Kalchenko, V.I. Kalchenko, S.V. Komisarenko, Calix 4 arene methylenebisphosphonic acids as inhibitors of fibrin polymerization, FEBS J. 278 (8) (2011) 1244–1251.
[69] H. Miyachi, J.W. Reinhardt, S. Otsuru, S. Tara, H. Nakayama, T. Yi, Y.U. Lee, S. Miyamoto, T. Shoji, T. Sugiura, C.K. Breuer, T. Shinoka, Bone marrow-derived mononuclear cell seeded bioresorbable vascular graft improves acute graft patency by inhibiting thrombus formation via platelet adhesion, Int. J. Cardiol. 266 (2018) 61–66.
[70] Z. Yang, Q. Tu, M.F. Maitz, S. Zhou, J. Wang, N. Huang, Direct thrombin inhibitor-bivalirudin functionalized plasma polymerized allylamine coating for improved biocompatibility of vascular devices, Biomaterials 33 (32) (2012) 7959–7971.
[71] S.W. Jordan, E.L. Chaikof, Novel thromboresistant materials, J. Vasc. Surg. 45 (2007) 104A–115A.
[72] R.A. Campbell, K.A. Overmyer, C.R. Bagnell, A.S. Wolberg, Cellular procoagulant activity dictates clot structure and stability as a function of distance from the cell surface, Arterioscler. Thromb. Vasc. Biol. 28 (12) (2008) 2247–2254.
[73] R.A. Campbell, K.A. Overmyer, C.H. Selzman, B.C. Sheridan, A.S. Wolberg, Contributions of extravascular and intravascular cells to fibrin network formation, structure, and stability, Blood 114 (23) (2009) 4886–4896.
[74] S. Kattula, J.R. Byrnes, A.S. Wolberg, Fibrinogen and fibrin in hemostasis and thrombosis, Arterioscler. Thromb. Vasc. Biol. 37 (3) (2017) E13–E21.
[75] P. Gao, H. Qiu, K. Xiong, X. Li, Q. Tu, H. Wang, N. Lyu, X. Chen, N. Huang, Z. Yang, Metal-catechol-(amine) networks for surface synergistic catalytic modification: therapeutic gas generation and biomolecule grafting, Biomaterials 248 (2020), 119981.
[76] Z. Yang, Q. Tu, Y. Zhu, R. Luo, X. Li, Y. Xie, M.F. Maitz, J. Wang, N. Huang, Mussel-inspired coating of polydopamine directs endothelial and smooth muscle cell fate for re-endothelialization of vascular devices, Adv. Healthc. Mater. 1 (5) (2012) 548–559.
[77] Y. Ma, L. Jiang, J. Hu, H. Liu, S. Wang, P. Zuo, P. Ji, L. Qu, T. Cui, Multifunctional 3D micro-nanostructures fabricated through temporally shaped femtosecond laser processing for preventing thrombosis and bacterial infection, ACS Appl. Mater. Interfaces 12 (15) (2020) 17155–17166.
[78] C. Kimmelstiel, P. Zhang, N.K. Kapur, A. Weintraub, B. Krishnamurthy, V. Castaneda, L. Covic, A. Kuliopulos, Bivalirudin is a dual inhibitor of thrombin and collagen-dependent platelet activation in patients undergoing percutaneous coronary intervention, Circ. Cardiovasc. Interv. 4 (2) (2011) 171–179.
[79] H. Qiu, Q.F. Tu, P. Gao, X.Y. Li, M.F. Maitz, K.Q. Xiong, N. Huang, Z.L. Yang, Phenolic-amine chemistry mediated synergistic modification with polyphenols and thrombin inhibitor for combating the thrombosis and inflammation of cardiovascular stents, Biomaterials 269 (2021), 120626.
[80] Y. Yang, X.Y. Li, H. Qiu, P. Li, P.K. Qi, M.F. Maitz, T.X. You, R. Shen, Z.L. Yang, W. J. Tian, N. Huang, Polydopamine modified TiO2 nanotube arrays for long-term controlled elution of bivalirudin and improved hemocompatibility, ACS Appl. Mater. Interfaces 10 (9) (2018) 7649–7660.
[81] N. Dahan, U. Sarig, T. Bronshtein, L. Baruch, T. Karram, A. Hoffman, M. Machluf, Dynamic autologous reendothelialization of small-caliber arterial extracellular matrix: a preclinical large animal study, Tissue Eng. 23 (1–2) (2017) 69–79.
[82] T.C. Ren, S. Yu, Z.W. Mao, S.E. Moya, L.L. Han, C.Y. Gao, Complementary density gradient of poly(hydroxyethyl methacrylate) and YIGSR selectively guides migration of endotheliocytes, Biomacromolecules 15 (6) (2014) 2256–2264.
[83] S. Yu, Y. Gao, X. Mei, T.C. Ren, S. Liang, Z.W. Mao, C.Y. Gao, Preparation of an Arg-Glu-Asp-Val peptide density gradient on hyaluronic acid-coated poly(epsilon-caprolactone) film and its influence on the selective adhesion and directional migration of endothelial cells, ACS Appl. Mater. Interfaces 8 (43) (2016) 29280–29288.
[84] W.J. Seeto, Y. Tian, E.A. Lipke, Peptide-grafted poly(ethylene glycol) hydrogels support dynamic adhesion of endothelial progenitor cells, Acta Biomater. 9 (9) (2013) 8279–8289.
[85] D. Hao, W.W. Xiao, R.W. Liu, P. Kumar, Y.P. Li, P. Zhou, F.Z. Guo, D.L. Farmer, K. S. Lam, F.S. Wang, A.J. Wang, Discovery and characterization of a potent and specific peptide ligand targeting endothelial progenitor cells and endothelial cells for tissue regeneration, ACS Chem. Biol. 12 (4) (2017) 1075–1086.
[86] A.A. Shitole, P.S. Giram, P.W. Raut, P.P. Rade, A.P. Khandwekar, N. Sharma, B. Garnaik, Clopidogrel eluting electrospun polyurethane/polyethylene glycol thromboresistant, hemocompatible nanofibrous scaffolds, J. Biomater. Appl. 33 (10) (2019) 1327–1347.
[87] H. Kuang, S. Yang, Y. Wang, Y. He, K. Ye, J. Hu, W. Shen, Y. Morsi, S. Lu, X. Mo, Electrospun bilayer composite vascular graft with an inner layer modified by polyethylene glycol and haparin to regenerate the blood vessel, J. Biomed. Nanotechnol. 15 (1) (2019) 77–84.
[88] W.S. Choi, Y.K. Joung, Y. Lee, J.W. Bae, H.K. Park, Y.H. Park, J.-C. Park, K. D. Park, Enhanced patency and endothelialization of small-caliber vascular grafts fabricated by coimmobilization of heparin and cell-adhesive peptides, ACS Appl. Mater. Interfaces 8 (7) (2016) 4336–4346.
[89] S.E. Sakiyama-Elbert, J.A. Hubbell, Development of fibrin derivatives for controlled release of heparin-binding growth factors, J. Contr. Release 65 (3) (2000) 389–402.
[90] E.J. Walker, C.K. Pandiyarajan, K. Efimenko, J. Genzer, Generating surface-anchored zwitterionic networks and studying their resistance to bovine serum albumin adsorption, ACS Appl. Polym. Mater. 1 (12) (2019) 3323–3333.
[91] R. Xu, X.Z. Cui, Q.W. Xin, M. Lu, Z.Q. Li, J.S. Li, X.Y. Chen, Zwitterionic PMCP-functionalized titanium surface resists protein adsorption, promotes cell adhesion, and enhances osteogenic activity, Colloids Surf. B Biointerfaces 206 (2021), 111928.
[92] S.G. Boswell, B.J. Cole, E.A. Sundman, V. Karas, L.A. Fortier, Platelet-rich plasma: a milieu of bioactive factors, Arthroscopy 28 (3) (2012) 429–439.
[93] T. Burnouf, H.A. Goubran, T.M. Chen, K.L. Ou, M. El-Ekiaby, M. Radosevic, Blood-derived biomaterials and platelet growth factors in regenerative medicine, Blood Rev. 27 (2) (2013) 77–89.
[94] Y. Wei, Y. Ji, L.L. Xiao, Q.K. Lin, J.P. Xu, K.F. Ren, J. Ji, Surface engineering of cardiovascular stent with endothelial cell selectivity for in vivo re-endothelialisation, Biomaterials 34 (11) (2013) 2588–2599.
[95] J.C. Deng, S.H. Yuan, J. Wang, R.F. Luo, S. Chen, J. Wang, N. Huang, Fabrication of endothelial progenitor cell capture surface via DNA aptamer modifying dopamine/polyethyleneimine copolymer film, Appl. Surf. Sci. 386 (2016) 138–150.
[96] H. Qiu, P.K. Qi, J.X. Liu, Y. Yang, X. Tan, Y. Xiao, M.F. Maitz, N. Huang, Z. L. Yang, Biomimetic engineering endothelium-like coating on cardiovascular stent through heparin and nitric oxide-generating compound synergistic modification strategy, Biomaterials 207 (2019) 10–22.
[97] A.J. Melchiorri, N. Hibino, T. Yi, Y.U. Lee, T. Sugiura, S. Tara, T. Shinoka, C. Breuer, J.P. Fisher, Contrasting biofunctionalization strategies for the enhanced endothelialization of biodegradable vascular grafts, Biomacromolecules 16 (2) (2015) 437–446.
[98] K. Wang, Q. Zhang, L. Zhao, Y. Pan, T. Wang, D. Zhi, S. Ma, P. Zhang, T. Zhao, S. Zhang, W. Li, M. Zhu, Y. Zhu, J. Zhang, M. Qiao, D. Kong, Functional modification of electrospun poly(epsilon-caprolactone) vascular grafts with the fusion protein VEGF-HGFI enhanced vascular regeneration, ACS Appl. Mater. Interfaces 9 (13) (2017) 11415–11427.
[99] D. Hao, Y. Fan, W. Xiao, R. Liu, C. Pivetti, T. Walimbe, F. Guo, X. Zhang, D. L. Farmer, F. Wang, A. Panitch, K.S. Lam, A. Wang, Rapid endothelialization of small diameter vascular grafts by a bioactive integrin-binding ligand specifically targeting endothelial progenitor cells and endothelial cells, Acta Biomater. 108 (2020) 178–193.
[100] P.F. Sanchez, E.M. Brey, J. Carlos Briceno, Endothelialization mechanisms in vascular grafts, J. Tissue Eng. Regen. Med. 12 (11) (2018) 2164–2178.
[101] T.R. He, T.E. Peterson, Z.S. Katusic, Paracrine mitogenic effect of human endothelial progenitor cells: role of interleukin-8, Am. J. Physiol. Heart Circ. Physiol. 289 (2) (2005) H968–H972.
[102] D. Burger, J.L. Vinas, S. Akbari, H. Dehak, W. Knoll, A. Gutsol, A. Carter, R. M. Touyz, D.S. Allan, K.D. Burns, Human endothelial colony-forming cells protect against acute kidney injury : role of exosomes, Am. J. Pathol. 185 (8) (2015) 2309–2323.
[103] M. Valgimigli, H. Bueno, R.A. Byrne, J.P. Collet, F. Costa, A. Jeppsson, P. Juni, A. Kastrati, P. Kolh, L. Mauri, G. Montalescot, F.J. Neumann, M. Petricevic, M. Roffi, P.G. Steg, S. Windecker, J.L. Zamorano, G.N. Levine, L. Badimon, P. Vranckx, S. Agewall, F. Andreotti, E. Antman, E. Barbato, J.P. Bassand, R. Bugiardini, M. Cikirikcioglu, T. Cuisset, M. De Bonis, V. Delgado, D. Fitzsimons, G. Oliver, N. Galie, M. Gilard, C.W. Hamm, B. Ibanez, B. Iung, S. James, J. Knuuti, U. Landmesser, C. Leclercq, M. Lettino, G. Lip, M.F. Piepoli, L. Pierard, M. Schwerzmann, U. Sechtem, I.A. Simpson, M.S. Uva, E. Stabile, R. F. Storey, M. Tendera, F. Van De Werf, F. Verheugt, V. Aboyans, T. Task Force Dual Antiplatelet, S. European Asso Cardio-Thoracic, ESC focused update on dual antiplatelet therapy in coronary artery disease developed in collaboration with EACTS, Eur. Heart J. 39 (3) (2017) 213–260, 2018.
[104] B.E. Thames, J. Lovvorn, M.G. Papich, R. Wills, T. Archer, A. Mackin, J. Thomason, The effects of clopidogrel and omeprazole on platelet function in normal dogs, J. Vet. Pharmacol. Therapeut. 40 (2) (2017) 130–139.
[105] N. McLewee, T. Archer, R. Wills, A. Mackin, J. Thomason, Effects of aspirin dose escalation on platelet function and urinary thromboxane and prostacyclin levels in normal dogs, J. Vet. Pharmacol. Therapeut. 41 (1) (2018) 60–67.
[106] J.M. Haines, J.M. Thomason, E.C. Seage, R.W. Wills, C. Bulla, K.V. Lunsford, A. J. Mackin, Vitro and in vivo assessment of platelet function in healthy dogs during administration of a low-dose aspirin regimen, Am. J. Vet. Res. 77 (2) (2016) 174–185.
[107] T. Sugiura, G. Matsumura, S. Miyamoto, H. Miyachi, C.K. Breuer, T. Shinoka, Tissue-engineered vascular grafts in children with congenital heart disease: intermediate term follow-up, Semin. Thorac. Cardiovasc. Surg. 30 (2) (2018) 175–179.
[108] S.L. Blois, D.G. Allen, R.D. Wood, P.D. Conlon, Effects of aspirin, carprofen, deracoxib, and meloxicam on platelet function and systemic prostaglandin concentrations in healthy dogs, Am. J. Vet. Res. 71 (3) (2010) 349–358.
[109] D. Sharma, D. Ross, G. Wang, W. Jia, S.J. Kirkpatrick, F. Zhao, Upgrading prevascularization in tissue engineering: a review of strategies for promoting highly organized microvascular network formation, Acta Biomater. 95 (2019) 112–130.

[110] S. Kargozar, F. Baino, S. Hamzehlou, R.G. Hill, M. Mozafari, Bioactive Glasses: sprouting angiogenesis in tissue engineering, Trends Biotechnol. 36 (4) (2018) 430–444.
[111] Y. Shang, D. Zhi, G. Feng, Z. Wang, D. Mao, S. Guo, R. Liu, L. Liu, S. Zhang, S. Sun, K. Wang, D. Kong, J. Gao, Z. Yang, Supramolecular nanofibers with superior bioactivity to insulin-like growth factor-I, Nano Lett. 19 (3) (2019) 1560–1569.
[112] D.M. Headen, K.B. Woodward, M.M. Coronel, P. Shrestha, J.D. Weaver, H. Zhao, M. Tan, M.D. Hunckler, W.S. Bowen, C.T. Johnson, L. Shea, E.S. Yolcu, A. J. Garcia, H. Shirwan, Local immunomodulation with Fas ligand-engineered biomaterials achieves allogeneic islet graft acceptance, Nat. Mater. 17 (8) (2018) 732–739.